Signals from the head and germinative region differentially regulate regeneration competence of the tapeworm *Hymenolepis diminuta*.

Elise McCollough Nanista[1], Landon Elizabeth Poythress[1], Isabell Reese Skipper[1], Trevor Haskins[1], Marieher Felix Cora[2] and Tania Rozario[1]*

[1]University of Georgia, Athens, GA, USA

[2]University of Puerto Rico-Cayey, PR, USA

Running title: Tapeworm regeneration competence

* corresponding author

tania.rozario@uga.edu

500 D.W. Brooks Dr., Athens, GA 30602, USA

ORCIDS:

EMN: 0009-0002-3844-876X

LEP: 0009-0007-5836-5714

IRS: 0009-0009-1869-7292

TH: 0009-0007-1528-3807

MFC: 0009-0004-9971-0826

TR: 0000-0002-9971-5211

Keywords: regeneration, tapeworm, planaria, flatworm, Wnt signaling

Abstract

Competence to regenerate lost tissues varies widely across species. The rat tapeworm, *Hymenolepis diminuta*, undergoes continual cycles of shedding and regenerating thousands of reproductive segments to propagate the species. Despite its prowess, *H. diminuta* can only regenerate posteriorly from a singular tissue: the neck or germinative region (GR). What cells and signaling pathways restrict regeneration competence to the GR? In this study, we show that the head regulates regeneration competence by promoting maintenance of the GR and inhibiting proglottid formation in a distance-dependent manner. Anterior-posterior (A-P) patterning within the GR provide local signals that contribute to these responses. *βcat1* is necessary for stem cell maintenance, proliferation and proglottidization. On the other hand, *sfrp* is necessary for maintaining the GR at its proper length. Our study demonstrates that the head organizes a balance of pro- and anti-regeneration signals that must be integrated together and therefore control competence to regenerate.

Summary statement

This study explores contradictory roles of the tapeworm head in providing pro- and anti-regeneration signals, which can form a tipping point zone that is refractory to regeneration.

Introduction

Regeneration occurs over a wide range of biological scales from regeneration of axons at the cellular scale to whole body regeneration in planarians and hydra (Bely and Nyberg, 2010). Tapeworms represent a fascinating case study in regeneration. They descend from a monophyletic clade (Neodermata) exclusively populated by parasites within the Platyhelminthes phylum (Laumer et al., 2015). As a sister group to planarians, it is possible that shared regenerative abilities have enabled tapeworms to achieve their monstrous growth potential and reproductive prowess. Many species of intestinal tapeworms shed large pieces of their body to disperse the developing embryos for consumption by an intermediate host, while continuously replenishing the lost tissue. Studies with the rat tapeworm, *Hymenolepis diminuta*, demonstrated that anterior fragments regenerated reproductive segments (proglottids) after serial rounds of amputation and transplantation into new host intestines for over a decade (Goodchild, 1958; Read, 1967). This greatly prolonged the normal lifespan of *H. diminuta* suggesting that this parasite may not inherently need to age and die.

By culturing *H. diminuta in vitro*, we were able to determine its range of regenerative abilities (Rozario et al., 2019) (Fig. 1A). Head regeneration was never observed. Posterior regeneration of new proglottids occurred but only when the neck/germinative region (GR) was retained. Neither the head nor proglottids could regenerate new proglottids. Hence, the GR is the only regeneration-competent tissue. We confirmed that similar to the serial transplantation experiments described above, 2 mm anterior fragments of *H. diminuta* regenerated proglottids after serial rounds of amputation and growth *in vitro*. However, proglottid regeneration was finite when the head region was removed indicating that persistent regeneration does require head-dependent signals.

Proglottid regeneration depends on GR-resident stem cells, but this population is not functionally unique (Rozario et al., 2019). When stem cells were depleted by a lethal dose of irradiation, proglottid regeneration from the GR was inhibited. Transplantation of donor cells into irradiated GRs rescued regeneration, as long as cycling stem cells were present in the donor pool. Interestingly, the rescue occurred with donor cells from the GR as well as with donor cells from

73 regeneration-incompetent parts of the body. Hence, while stem cells are necessary for
74 regeneration, signals within the GR are paramount.
75
76 A plethora of unknown signals likely operate in the GR and control stem cell proliferation,
77 survival, differentiation, as well as proglottidization and competence to regenerate. Here we show
78 that regeneration competence is tightly linked to signals from the head. The head plays seemingly
79 contradictory roles as it is necessary to maintain the GR but negatively regulates proliferation and
80 proglottid regeneration. We find two genes typically associated with Wnt signaling, *βcatenin1* and
81 *sfrp*, as critical mediators of stem cell maintenance and GR length, respectively. Our study
82 demonstrates that a balance of pro- and anti-regeneration signals must be overcome to enable GR
83 regeneration and then initiation of proglottids. *H. diminuta* provides a fascinating example of how
84 extrinsic signals can promote or restrict the ability to regenerate.

Results

H. diminuta can regenerate the GR.

Anterior fragments containing the head, GR and a few immature proglottids are competent to regenerate new proglottids (Rozario et al., 2019). However, it is unclear if the GR can regenerate itself and subsequently proglottidize. After acclimating worms to *in vitro* culture conditions for 3 days, we amputated within the GR (0.5 mm) vs. outside the GR (2 mm) and grew the anterior fragments for 15 days. In both cases, proglottids regenerated (Fig. 1B). At 15 dpa, GR lengths in regenerates from both groups were comparable at 1.01±0.08 mm and 1.07±0.05 mm (Fig. 1C). The 0.5 mm fragments regenerated GRs within 2-4 days before new proglottids were added (Fig. 1D). The rate of proglottid regeneration was comparable between both fragment types, at 14-15 proglottids per day (Fig. 1D). Thus, when amputated within the GR, *H. diminuta* is capable of regenerating the posterior GR and subsequently proglottids.

The GR is patterned by differentially expressed genes along the anterior-posterior (A-P) axis (Rozario et al., 2019). If *H. diminuta* can regenerate its GR, then A-P polarized patterns should be restored following amputation. We performed whole mount *in situ* hybridization (WISH) for three posterior-enriched transcripts: *βcatenin1* (*βcat1;* WMSIL1_LOCUS14475), *frizzled5/8* (*fzd5/8;* WMSIL1_LOCUS9542), and *tumor necrosis factor receptor-16* (*tnfr16;* WMSIL1_LOCUS10339) and one anterior-enriched transcript: *secreted frizzled related protein* (*sfrp;* WMSIL1_LOCUS14856) (Fig. 1E; uncut). The antisense riboprobes used showed distinct patterns while matched sense riboprobes showed minimal background (Fig. S1). Worms were amputated within the GR (0.5 mm) and at 0 dpa, all markers were reduced or lost (Fig. 1E). A-P polarized patterns were restored by at least 10 dpa demonstrating normal GR patterning (Fig. 1E).

GR regeneration fails after serial amputation.

We investigated if GR regeneration occurs after serial amputation. Newly harvested worms were acclimated *in vitro* for 3 days, 0.5 mm anterior fragments were obtained (cut 1) and grown for 18 days before re-amputation (cut 2) (Fig. 2A). Subsets of each group were fixed to capture the variation and reproducibility of the amputations performed. We find that tissues extend slightly after heat-killing and fixation resulting in slightly longer 0 dpa fragments: 0.63±0.07 mm and 0.61±0.16 mm after each amputation (Fig. 2B; means). While fragment length did vary there was

116 no statistically significant difference at each timepoint. The GR lengths were longer at cut 1
117 (1.32±0.11 mm) than at cut 2 (1.09±0.08 mm) yet the percentage of GR length retained was close
118 to the target range of 50% and the mean differences were not statistically significant (48±9% after
119 cut 1 and 56±11% after cut 2) (Fig. 2C; means). When pooled together, there was a bias toward
120 increased % of GR length retained after cut 2 (Fig. 2C; all), indicating that despite our best efforts,
121 the average amputation position in the GR may have been slightly different between the two
122 timepoints. After cut 1, almost all fragments regenerated GRs and proglottids (Fig. 2D). After cut
123 2, many fragments failed to regenerate at all producing inconsistent regeneration rates per
124 experiment (Fig. 2D). Worms that did regenerate after cut 2 were significantly shorter (Fig. 2E)
125 and produced fewer proglottids (Fig. 2F). Thus, GR regeneration can fail under certain conditions.
126
127 **Signals from the head regulate proglottid regeneration and GR maintenance.**
128 When amputating within the GR, the wound site is closer to the head. We suspected that the head
129 asserts a negative effect on regeneration. After head amputation, regenerates exhibited increased
130 growth and proglottid regeneration (Fig. 3A) indicating that signals from the head do inhibit
131 growth. Using 1 hr uptake of the thymidine analog F-*ara*-EdU (Neef and Luedtke, 2011) to
132 quantify the density of proliferating cells in the GR, we found that head amputation increased
133 proliferation, which can explain the increased growth (Fig. 3B). In uncut worms, proliferation
134 density in the GR increases with distance from the head (Fig. 3C) further supporting our conclusion
135 that the head provides anti-proliferation signals. Upon head amputation and *in vitro* culture for 3
136 days, the increasing proliferation density along the GR A-P axis was no longer significant (Fig.
137 3D). However, the curves did not fully flatten. While signals from the head do regulate
138 proliferation in the GR, the effects are slow to dissipate or mediated by additional factors resident
139 within the GR.
140
141 Many regenerating animals respond to wounding by increasing proliferation locally. Following
142 amputation in the GR, we quantified proliferation at both anterior- and posterior-facing wounds
143 and found increased proliferation (Fig. S2). However, the local increase in proliferation was
144 equivalent regardless of head presence (Fig. S2). Thus, amputation itself does not explain the
145 increased proliferation in -head worms but could contribute to increased proliferation.
146

147 Previous results have shown that GR maintenance depends on the head; after head amputation, the
148 GR is eventually lost, the regenerates become fully proglottidized and cannot continue adding
149 proglottids (Rozario et al., 2019). To further characterize how the head affects proglottid
150 regeneration and GR maintenance, four amputation schemes were compared: + head, ½ head, -
151 head, and -0.5 mm anterior (Fig. 4A). Making transverse cuts through the head was technically
152 challenging so a sampling of ½ head fragments were fixed immediately and stained with anti-
153 SYNAPSIN antibodies to visualize the nervous system. Though the amount of head tissue
154 removed did vary, the brain was always retained (Fig. S3A: yellow arrowheads). After making the
155 four different amputations at the anterior region, we assayed proglottid regeneration following
156 serial amputation. All worms were amputated posteriorly to obtain fragments of the same length
157 (2 mm), that were grown *in vitro* for 14 days, then re-amputated for 3 more cycles (Fig. 4A). The
158 posteriors were collected to determine the number of proglottids regenerated after every cycle. As
159 previously reported (Rozario et al., 2019), tapeworms regenerated after serial amputation when the
160 head was present (Fig. 4B). The ½ head regenerates consistently displayed increased proglottid
161 regeneration compared to +head regenerates (Fig. 4B). Both +head and ½ head regenerates
162 maintained their GRs throughout 2 months of *in vitro* culture. When the head was amputated
163 completely (-head), proglottid regeneration eventually ceased though some regenerates still had
164 GRs after the 4th amputation (Fig. 4B). These -head regenerates had significantly shorter GRs (Fig.
165 S3B) indicating that complete proglottidization was imminent. Previously, we observed rapid loss
166 of the GR after head amputation, but anterior GR tissue was also removed in those experiments
167 (Rozario et al., 2019). In this study, we were careful to make minimal head amputations that
168 retained as much anterior GR and found that the GR persists for much longer than previously
169 reported but does eventually recede. On the other hand, fragments in which both the head and
170 anterior GR were removed (-0.5 mm) became fully proglottidized by the second amputation or
171 earlier (Fig. 4B). In sum, GRs were maintained if the brain region was retained but GRs were lost
172 when additional anterior tissue was removed (Fig. 4C).
173
174 The number of proglottids regenerated also depended on amputations at the head though our
175 analysis was complicated by GR loss in -head and -0.5mm fragments. After the first amputation,
176 a clear dose-dependent response was detected; when more head tissue was retained, the number of
177 proglottids decreased (Fig. S3C). This trend was maintained after serial rounds of amputation when

178 comparing +head and ½ head regenerates where GRs were not lost (Fig. S3D). After the 4th round
179 of amputation, the remaining head area plotted against number of proglottids for +head and ½ head
180 regenerates revealed a negative correlation between head tissue abundance and proglottidization
181 (Fig. 4D). We also measured the effect of head tissue abundance on proliferation within the GR
182 using F-*ara*-EdU. A general trend of increasing proliferation with decreasing head and anterior
183 tissue emerged though differences between +head and ½ head were not statistically significant
184 (Fig. 4E-F). Taken together, the head effects on maintaining the GR and regulating proliferation
185 can be separated. Signals from the brain region are necessary to maintain the GR whereas
186 proliferation and proglottidization are negatively regulated by head-dependent signals in a dose-
187 dependent manner.
188
189 ***βcatenin1* is necessary for proglottid regeneration and stem cell maintenance.**
190 To begin to ascertain the molecular regulators of GR maintenance, stem cell proliferation and
191 proglottid regeneration rate, we turned to the Wnt signaling pathway. Wnt signaling determines
192 A-P polarity in many systems (Petersen and Reddien, 2009) and plays roles in regulating cell
193 proliferation, survival, and differentiation (Nusse and Clevers, 2017). Expression of multiple
194 members of the Wnt signaling pathway were either anterior-enriched or posterior-enriched by
195 RNA sequencing along the A-P axis of the GR (Rozario et al., 2019). As βcatenin protein is a key
196 downstream effector of Wnt signaling, we decided to examine its function. *H. diminuta* has three
197 *βcatenin* paralogs as do other parasitic flatworms (Montagne et al., 2019). BLASTp comparisons
198 of putative *H. diminuta βcatenin* paralogs with published sequences for other flatworms
199 (*Schmidtea mediterranea*, *Schistosoma mansoni* and *Echinococcus multilocularis*) demonstrated
200 that *Hdim-βcat1* (WMSIL1_LOCUS14475) is the rat tapeworm ortholog of *βcat1* (Table S1).
201 Expected conserved domains including multiple armadillo repeats and the DSGxxSxxx[S/T]xxxS
202 motif for CKI/GSK-phosphorylation necessary for targeting by the destruction complex
203 (Montagne et al., 2019; Valenta et al., 2012) are present (Fig. S4A). Capacity to bind α-catenin
204 cannot be ruled in or out at present (Fig. S4B; discussed below). Thus *Hdim-βcat1* likely mediates
205 Wnt signaling and may also function in cell adhesion.
206
207 In 6-day-old adults, *Hdim-βcat1* (hereafter *βcat1*) expression is largely absent in the head and
208 anterior GR but increases toward the posterior GR (Fig. 5A). *βcat1* is broadly expressed in many

209 tissues, in transverse stripes at proglottid boundaries and within accessory reproductive structures
210 (Fig. S5). We injected double-stranded RNA (dsRNA) targeting *βcat1* throughout the GR and
211 grew 2 mm anterior fragments *in vitro*. A dramatic growth defect was captured just 7 dpa/10 days
212 post injection (dpi) (Fig. 5B). Decreased growth was evident by 3 dpa and this RNAi treatment
213 was ultimately lethal. The proglottids formed were extremely small and impossible to quantify but
214 there was a marked decrease in worm lengths (Fig. 5C). RNAi of *βcat1* reduced transcript levels
215 to 8.7±2.0% (Fig. 5D). In canonical Wnt signaling, *βcat1* is a transcription factor with many targets
216 including *axins*, though *bona fide* targets in tapeworms have not been determined. Tapeworm *axins*
217 are highly divergent, but previous work using exogenous expression of AXIN1 and AXIN2 from
218 the fox tapeworm *E. multilocularis,* showed evidence that both AXINs function canonically in the
219 Wnt signaling pathway (Montagne et al., 2019). In *H. diminuta*, *axin1* (WMSIL1_LOCUS3986)
220 is broadly expressed in overlapping patterns with *βcat1* whereas *axin2* (WMSIL1_LOCUS6411)
221 is highly tissue-specific (Fig. S5). After *βcat1* RNAi, *axin1* expression is markedly reduced to
222 18.8±11.1% of normal levels (Fig. 5D). This suggests that canonical Wnt signaling is inhibited
223 following *βcat1* RNAi though other roles for *βcat1* cannot be ruled out.
224
225 Given the strong decrease in growth after *βcat1* RNAi, we hypothesized that cycling stem cells
226 require *βcat1*. Proliferation was significantly decreased in *βcat1* RNAi GRs compared to *GFP*
227 RNAi controls (Fig. 5E). WISH for two known stem cell markers in *H. diminuta*: *minichromosome*
228 *maintenance complex component-2* (*mcm2;* WMSIL1_LOCUS11918) and *laminB receptor* (*lbr;*
229 WMSIL1_LOCUS1236) (Rozario et al., 2019) showed decreased expression after *βcat1* RNAi
230 (Fig. 5F). Thus, *βcat1* is required to maintain stem cells in the GR through regulation of
231 proliferation and/or other mechanisms.
232
233 **GR maintenance requires *sfrp*.**
234 We hypothesized that *βcat1* activity may be counterbalanced by anterior-localized Wnt inhibitors.
235 Previous RNA-sequencing analyses showed that *sfrp* expression is enriched in the anterior GR
236 (Rozario et al., 2019). Like other tapeworms, *H. diminuta* has one true *sfrp* family member and a
237 second highly divergent member, *sfrp-like* (WMSIL1_LOCUS8400), which was not investigated
238 further in this study. Interpro (Blum et al., 2020) predicts that Hdim-SFRP retains both frizzled

239 and netrin domains albeit with some variation (Fig. S6; discussed below). Since SFRP can inhibit
240 Wnt signaling (Leyns et al., 1997; Rattner et al., 1997; Wang et al., 1997), we pursued its potential
241 role in regeneration.
242
243 By WISH, *sfrp* expression is strikingly anterior-enriched with sparce expression in the head and
244 strong expression throughout the GR that tapers off posteriorly (Fig. 6A). In adult tapeworms, *sfrp*
245 expression is largely absent from the strobilated body except at lateral ends of proglottids (Fig.
246 S5). We hypothesized that *sfrp* RNAi would promote proglottid regeneration as opposed to *βcat*
247 RNAi, which reduced proglottid regeneration. We injected *sfrp* dsRNA into the head, amputated
248 2 mm anterior fragments, reinjected dsRNA into the head and collected worms at 10-12 dpa (Fig.
249 6B). Contrary to our expectations, a modest decrease in worm lengths and proglottid regeneration
250 were observed (Fig. 6C-D). Strikingly, the GRs were significantly shortened following *sfrp* RNAi
251 (Fig. 6E-F). This is the first time GR length has been affected by RNAi of any target gene. Injecting
252 dsRNA into the head does not preclude diffusion into the GR but the knockdown is likely to be
253 anteriorly biased. We injected dsRNA throughout the GR and observed the same phenotypes (Fig.
254 S7A-C). Both injection schemes resulted in similar *sfrp* knockdown efficacy (Fig. S7D).
255
256 Our results indicate that *sfrp* is necessary for proper GR maintenance but is unlikely to be involved
257 in head-dependent inhibition of proliferation or proglottidization. Instead, *sfrp* could mediate head-
258 dependent GR maintenance. Upon head amputation, we observed a modest 32.2±14.0% decrease
259 in *sfrp* expression 3 days after head amputation (Fig. S7E). By WISH, the domain of *sfrp*
260 expression after head amputation was often reduced as the GR shrinks though it was highly
261 variable at 3 dpa (Fig. S7F). Head amputation does not acutely abolish *sfrp* expression but may be
262 required for long-term stable expression of *sfrp* at the GR.
263
264 Decreased proglottid regeneration after *sfrp* RNAi does not support the hypothesis that *sfrp*
265 functions as a Wnt inhibitor. Proliferation within the GR was not significantly changed after *sfrp*
266 RNAi (Fig. S7G). However, the shortening of the GR would bring the posterior boundary of the
267 GR closer to the head. Thus, *sfrp* RNAi may indirectly exacerbate the anti-proglottidization effects
268 from the head.
269

Amputation distance from the head determines whether pro- or anti-regeneration signals dominate.

Given these results, we hypothesized that the regeneration failure we observed after serial amputation within the GR (Fig. 2) was precipitated when the posterior wound was too close to the head, which allowed the growth inhibitory effects of the head to dominate. To test this, anterior fragments were allowed to regenerate after 0.5 mm amputation within the GR and then cut a second time at 4 different distances from the head. All samples were cut at ~1mm, then subsets were progressively shaved closer toward the head (Fig. 7A; cuts A-D). Subsets of fragments were fixed at 0 dpa and we verified that cut A-D progressively retained 87±5%, 64±7%, 47±9%, and 22±4% of the GR (Fig. 7B). For each of three experiments, proglottid regeneration plummeted at either cut B or C (Fig. 7C). Groups with the lowest regeneration success corresponded to 0 dpa subsets where the posterior wound position clustered at ~60% GR length (Fig. 7C-D; matched colored arrows). This suggests that there is a tipping-point region within the GR that is refractory to regeneration following amputation. Surprisingly, the smallest fragments (cut D) regenerated equivalently to the longest fragments (cut A) (Fig. 7C-D and Fig. S7). Fragments from cut A and D achieved different absolute lengths at 18 dpa but the fold change in growth was comparable (Fig. 7E). There was no significant difference is GR length between regenerates from cut A or D (Fig. 7F). Thus, amputations within the GR can result in successful regeneration but not always, with more failed incidences when the wound site was at intermediate distances from the head. These results suggest that there are yet more signals to be uncovered that explain how regeneration is promoted and restricted in tapeworms.

291 **Discussion**

292

293 **A working model for GR and proglottid regeneration.**

294 We propose the following working model (Fig. 8) to synthesize our current findings. The head
295 provides signals that promote and restrict regenerative ability. These two roles can be separated
296 anatomically and through molecular regulators. Proliferation and proglottidization rate are
297 negatively regulated by the head in a dose-dependent and distance-dependent manner with
298 increased proliferation farther from the head. Stem cells and germ cells are the only proliferative
299 population in flatworms (Baguñà, 2012; Bolla and Roberts, 1971; Collins et al., 2013; Ishan et al.,
300 2025; Koziol et al., 2014) and proglottid regeneration is a stem cell-dependent process (Rozario et
301 al., 2019). We find that *βcat1* is expressed in a posterior-biased pattern at the GR and that RNAi
302 of *βcat1* results in loss of proliferative stem cells. We speculate that the head may produce direct
303 or indirect inhibitor(s) of unknown posterior signals that promote *βcat1* activity. Alternatively, the
304 head-dependent inhibitors of regeneration may act independently of *βcat1*. On the other hand, the
305 head positively regulates regeneration by promoting GR maintenance. Without the brain-region,
306 the GR is gradually lost and when the anterior GR is also removed, GR loss happens quickly.
307 RNAi of *sfrp* results in shortened GRs indicating that *sfrp* contributes to GR maintenance. While
308 *sfrp* expression is clearly anterior-enriched, it is unclear if *sfrp* expression is promoted/maintained
309 by signals from the head.

310

311 Taken together, our model provides an explanation for the highly mixed results in regeneration
312 outcomes when re-amputations were made within the GR. When the posterior wound site was far
313 enough from the inhibitors in the head, regeneration could occur. When the posterior wound site
314 was close to the head, we speculate that the targets of the head-dependent inhibitors were not
315 present. The head could promote proper growth of the GR, and at a sufficient distance from the
316 head, proglottids regenerated. However, when the posterior wound site was at intermediate
317 distances from the head, the inhibitors dominated leading to failure to regenerate. We speculate
318 that the pro- and anti-regeneration contributions of the head result in a tipping point zone that is
319 refractory to regeneration (Fig. 8). The exact players, direct and indirect relationships, as well as
320 additional molecular mechanisms predicted by our working model still need to be tested.
321 Alternatives to our model certainly exist. For example, GR and proglottid regeneration may occur

322 from a wide range of posterior amputation sites with sporadic failures. These failures may be
323 caused by anterior inhibitory signals that are not always sufficient to block regeneration. Future
324 experiments will help determine if regeneration in *H. diminuta* is largely stochastic or tightly
325 regulated by spatially distinct molecular interactions.
326
327 Why GR regeneration did not fail significantly after the first round of amputations is unclear.
328 Tapeworm dimensions change when grown *in vitro*. Despite acclimating worms *in vitro* for 3 days
329 before all amputations, the spatial distribution and concentration of factors from the head to GR
330 could have been different at cut 1 vs. cut 2 (Fig. 2). GR regeneration competence does not merely
331 dissipate over time as the smallest fragments (cut D) successfully regenerated proglottids and the
332 GR after the second round of amputation (Fig. 7). The head may be acting as an organizer that sets
333 up a signaling environment within the GR that impacts regeneration positively and negatively in
334 ways that we are just beginning to discover.
335
336 **Differing roles for *βcat1* in flatworm regeneration.**
337 In *H. diminuta*, *βcat1* is necessary to maintain stem cell abundance and RNAi of *βcat1* results in
338 a dramatic inhibition of growth, proglottid regeneration and ultimately death. In the liver fluke,
339 *Fasciola hepatica,* RNAi of *Fhep-βcat1* stunted juvenile growth, decreased proliferation and
340 caused worm death (Armstrong et al., 2025), phenocopying our observations. Thus, roles for *βcat1*
341 in regulating stem cell proliferation and/or survival may be a common theme in parasitic flatworms
342 as it is in many metazoans and in cancers (Mohammed et al., 2016; Steinhart and Angers, 2018) .
343
344 In addition to canonical Wnt signaling, β-catenin proteins function in cell adhesion through linking
345 cadherins with the actin cytoskeleton via α-catenin in many but not all species. In *S. mediterranea,*
346 there is complete separation of function by two catenin paralogs: Smed-βCAT1 mediates Wnt
347 signaling whereas Smed-βCAT2 mediates cell adhesion (Chai et al., 2010; Su et al., 2017).
348 Accordingly, Smed-βCAT1 does not have α-catenin binding sites (Chai et al., 2010; Su et al.,
349 2017). The presence/absence of α-catenin binding sites in βCAT1 from tapeworms is more
350 ambiguous. Previously, a likely α-catenin binding region demarcated by 10 putative critical
351 residues (Aberle et al., 1996; Pokutta and Weis, 2000) within a 26 amino acid span was identified

352 for βCAT1 and βCAT2 in flatworms (Montagne et al., 2019). When compared to human βcatenin
353 (CTNB1), we and others find strong conservation of this α-catenin binding region in βCAT2 from
354 multiple flatworms (Fig. S4B) (Montagne et al., 2019). While Smed-βCAT1 is clearly very
355 divergent at this site, two tapeworms (*H. diminuta* and *E. multilocularis*) show more similarity to
356 the human reference (Fig. S4B) (Montagne et al., 2019). Thus, we cannot rule out the possibility
357 that βCAT1 in tapeworms functions in both Wnt signaling and cell adhesion, unlike their free-
358 living counterparts.
359
360 The role of *βcat1* in posterior identity is well conserved across many taxa (Petersen and Reddien,
361 2009). In planarian species that are deficient in head regeneration, knockdown of *βcat1* rescues
362 head regeneration indicating that failure to regenerate the head in wild type worms was due to the
363 inability to overcome the posteriorizing effects of *βcat1* (Liu et al., 2013; Sikes and Newmark,
364 2013; Umesono et al., 2013). *H. diminuta* cannot regenerate its head and we initially assumed that
365 tapeworm *βcat1* would be acting in a homologous fashion to planarians. Because *βcat1* is required
366 for stem cell maintenance in *H. diminuta,* potential roles in posteriorization could not be
367 uncovered. RNAi manipulations of other Wnt signaling components that are beyond the scope of
368 this study will help reveal a more holistic understanding of Wnt signaling in this system. However,
369 tapeworms and planarians do differ in that *Smed-βcat1* does not appear to affect stem cells since
370 after RNAi and amputation, blastemas form and there is no growth defect (Gurley et al., 2008;
371 Iglesias et al., 2008; Petersen and Reddien, 2008).
372
373 The differences in utilization of *βcat1* between different species of platyhelminths is potentially
374 very interesting. Perhaps segregating functions in posteriorization vs. stem cell maintenance in *S.*
375 *mediterranea* has enabled nimble remodeling of axes that makes this species so remarkable at
376 regenerating from almost any fragment. Intestinal tapeworms need the suckers at the head to attach
377 to the intestinal wall. Thus, maintenance of the head and proglottid regeneration may not be easily
378 decoupled in tapeworms. Considering the wider role for βcatenin in regulating stem cell
379 proliferation and survival across metazoa, it would be easy to assume that planarian phenotype is
380 divergent. However, studies in the acoel *Hofstenia miamia*, a sister group to all bilaterians, show
381 that RNAi of *Hmia-βcat1* is necessary for maintaining posterior identity but functions in regulating

382 stem cells, proliferation, or growth are not supported (Srivastava et al., 2014; Tewari et al., 2019).
383 Thus, the planarian phenotype may be ancestral. A deeper understanding of how catenin paralogs
384 have functionally specialized may reveal how strategies to regulate axial identity and stem cell
385 proliferation/survival have evolved in regeneration-competent species.
386
387 **GR maintenance and the role of *sfrp*.**
388 The mechanism by which *sfrp* maintains the GR is unknown. While *sfrp* is primarily known as a
389 Wnt antagonist, it can bind and stimulate frizzled receptors, interact with other signaling pathways
390 and modulate cell-matrix interactions by binding integrins (Bovolenta et al., 2008; Mii and Taira,
391 2011). There is evidence that *sfrps* can stimulate Wnt and BMP signaling in the zebrafish retina
392 (Holly et al., 2014). In *Drosophila*, *sfrps* can modulate Wnt signaling in a biphasic manner:
393 inhibiting Wnt signaling when expressed at high levels while promoting Wnt signaling when
394 expressed at low levels (Üren et al., 2000). In *H. diminuta*, the *sfrp* RNAi phenotypes were not the
395 opposite of the *βcat1* RNAi phenotypes as one might predict if *sfrp* and *βcat1* were acting solely
396 as Wnt antagonist and Wnt effector respectively. In many flatworms, Wnt ligands are secreted
397 from both anterior and posterior domains (Armstrong et al., 2025; Koziol et al., 2016; Reddien,
398 2018; Soria et al., 2020). Expression of *sfrp* throughout the GR may be required as a permissive
399 signal to tune Wnt signaling to a moderately low level so that it can be acted upon differentially
400 by other modulators. It is also possible that *sfrp* modulates *βcat1* activity differentially in a
401 tissue/cell-specific manner that we have yet to uncover. Alternatively, *sfrp* may function
402 independently of Wnt signaling. Future studies investigating RNAi phenotypes of other
403 antagonists, ligands and frizzed receptors will help resolve if/how other Wnt signaling components
404 regulate GR maintenance.
405
406 Biochemical evidence for parasitic flatworm SFRP proteins as Wnt inhibitors has not been
407 confirmed though both frizzled and netrin domains are readily identifiable. There are conflicting
408 assertions as to whether all 6 conserved cysteine residues typically found in the netrin domain are
409 present (Armstrong et al., 2025; Koziol et al., 2016; Riddiford and Olson, 2011). We detect all 6
410 cysteine residues, but the 6th residue is displaced by three animo acids in flatworms, including free-
411 living *S. mediterranea,* but not humans (Fig. S6). *Smed-sfrp1* is generally accepted as a Wnt
412 inhibitor (Doddihal et al., 2024; Hill and Petersen, 2018; Reuter et al., 2015; Scimone et al., 2016;

413 Stückemann et al., 2017; Sureda-Gómez et al., 2015). Thus, it remains possible that a muted or
414 more ambiguous role in Wnt signaling by *sfrp1* is a shared feature in free-living and parasitic
415 flatworms.
416
417 **Rationales for A-P polarized signals regulating regeneration.**
418 Our work has revealed that a balance of opposing signals at the GR can determine regeneration
419 competence. It makes intuitive sense that initiation of proglottids must be inhibited close to the
420 head if the GR is to be maintained as an unsegmented tissue. A recent study from the mouse bile
421 duct tapeworm, *Hymenolepis microstoma,* has described discrete expression of Wnt and Hedgehog
422 signaling components in a signaling quartet (SQ) within the transition zone from GR to fully
423 elaborated proglottids (Jarero et al., 2024). It is possible the SQ initiates proglottid formation and
424 represents the unknown targets of head-dependent inhibitors predicted by our study. How the SQ
425 responds to head-dependent signals and vice versa is currently unknown and warrants future
426 investigation.
427
428 Our study also shows that regulation of proliferation dynamics is dependent on signals from the
429 head. While amputation-induced proliferation does occur in *H. diminuta*, the enduring increase in
430 proglottid regeneration after ½ head removal and dose-dependent effects of head tissue abundance
431 on proliferation all suggest that the head provides signals that downregulate proliferation. What
432 purpose do anti-proliferation signals serve in the GR? One intriguing possibility is that signals
433 from the head could differentially regulate stem cell potency, self-renewal, asymmetric division or
434 other cell cycle dynamics. There is already evidence for different cycling rates in stem cells of
435 parasitic flatworms (Herz et al., 2024; Wang et al., 2018). Future investigation will help us
436 understand how head-dependent signals may influence stem cell behaviors.
437
438 In short, the head and GR constitute a signaling environment that influences regeneration
439 competence. Furthermore, the anterior GR contains a minimal cohort of stem cells and extrinsic
440 signals that are required to regenerate the GR and seed new proglottids. Understanding these
441 signals could enrich our knowledge of how stem cells and regeneration are regulated in parasitic
442 flatworms and beyond.
443

444 **Study limitations**

445 Our study relies on RNAi, which cannot eliminate gene expression. We also use *in vitro* culture
446 conditions that necessarily deviate from conditions *in vivo*. How environmental signals influence
447 our results is unknown. We have also only explored the contributions of two genes and tapeworm
448 regeneration is likely to be a complex process involving interconnecting networks of interactions.

449 **Materials and Methods**

450

451 Animal care and use

452 The life cycle of *H. diminuta* was maintained in house using mealworm beetles (*Tenebrio molitor*)
453 and Sprague-Dawley rats for the larval and adult stages respectively. Rats were fed 200-400
454 infective cysticercoids by oral gavage in ~0.5 mL 0.85% NaCl. Typically, adult tapeworms were
455 collected 6 days post infection by euthanizing infected rats in a CO_2 chamber and flushing the
456 small intestine with 1X Hanks Balanced Salt Solution (HBSS: 21-023-CV; Corning). Rodent care
457 was performed in accordance with protocols approved by the Institutional Animal Care and Use
458 Committee (IACUC) of the University of Georgia (A2023 10-019-Y1-A0).

459

460 *In vitro* parasite culture

461 Tapeworms were harvested 6 days post-infection and acclimated to *in vitro* culture conditions for
462 3 days before any amputations were made. We used biphasic cultures as described before (Rozario
463 et al., 2019). 2.5X MEM essential amino acids (M5550; Sigma-Aldrich) was added to the liquid
464 culture: Working Hanks 4 [WH4: 1X HBSS (MT21023CV; Corning), 4 g/L glucose (158968;
465 Sigma-Aldrich), 1X antibiotic-antimycotic (15240062; Fisher)]. This ameliorated inconsistencies
466 between batches of blood used for culturing but was not strictly necessary.

467

468 Cloning genes for riboprobe and dsRNA synthesis

469 Cloning was performed as previously described (Collins et al., 2010). All primers and accessions
470 are described in Table S2. Plasmids are available upon request. Briefly, adult *H. diminuta* cDNA
471 was used to PCR amplify products that were ligated into pJC53.2 plasmid via TA cloning.
472 Riboprobes for *in situ* hybridization were generated by *in vitro* transcription reactions with either
473 T3 or SP6 RNA polymerase (Ishan et al., 2025) . For RNAi, dsRNA was generated as previously
474 described (Rouhana et al., 2013) using T7 RNA polymerase.

475

476 *In situ* hybridization and other staining

477 Heat-kills were performed by swirling tapeworms in 75°C water for a few seconds before fixing
478 (4% formaldehyde in Phosphate Buffered Saline with 0.3% TritonX-100 (PBSTx)) for 30 min-2
479 hr at room temperature or overnight at 4°C. Worms were either dehydrated into methanol and

480 stored (-30°C) or used directly for staining. For simple phenotyping of growth and regeneration,
481 worms were stained in 1 µg/mL DAPI (D9542; Sigma-Aldrich)/PBSTx overnight at 4°C and
482 cleared in mounting solution (80% glycerol/10 mM Tris pH7.5/ 1 mM EDTA) overnight before
483 mounting and imaging. Previously published methods were employed for *in situ* hybridization
484 (Rozario et al., 2019) and immunostaining (Rozario and Newmark, 2015). Anti-SYN antibodies
485 (3C11; Developmental Studies Hybridoma Bank) were used at 1:200 with Tyramide Signal
486 Amplification (TSA).
487
488 F-*ara*-EdU uptake and staining
489 F-*ara*-EdU pulses were performed in 0.1 µM F-*ara*-EdU (T511293; Sigma-Aldrich)/1%
490 DMSO/WH4 at 37°C for 1 hr. Staining was performed as previously described (Ishan et al., 2025)
491 with the following specifics: 1) 15 min proteinase-K digestion (10 µg/mL in 0.1% SDS/PBSTx)
492 and 2) 10 min TSA reaction. F-*ara*-EdU+ cells were quantified using Imaris (Oxford Instruments)
493 spot finder from 3D confocal z-stacks. Automatic spot discovery (with background subtraction)
494 was enabled then manually adjusted to label all visible spots without false positives. All F-*ara*-
495 EdU data is represented as densities by normalizing to the area of the quantified fields.
496
497 Imaging and image processing
498 Confocal imaging was performed on a Zeiss LSM 900 with the following objectives: 20X/Plan-
499 Apochromat/0.8 M27/FWD=0.55mm and 63X/Plan-Apochromat/1.40 Oil DIC M27. WISH and
500 DAPI-stained worms were imaged on a Zeiss AxioZoom V16 Microscope. Fiji (Schindelin et al.,
501 2012) was used for brightness/contrast adjustments, maximum-intensity projections and
502 measurements of lengths, areas, and numbers of proglottids.
503
504 RNAi
505 Knockdowns were performed as previously described (Rozario et al., 2019). Tapeworms were
506 microinjected with dsRNA (1-1.5 µg/µl in HBSS), 2 mm anterior fragments were amputated 3
507 days later and cultured *in vitro*. Injections were performed using a Femtojet 4i (Eppendorf) at 500
508 hPa for 0.3-1s. Injection of *GFP* dsRNA (Roberts-Galbraith et al., 2016) was used as a negative
509 control. Experimenters were blinded to the dsRNA used throughout microinjections, staining and
510 image analysis.

511

512 qRT-PCR

513 To exclude genomic DNA, primers were designed to flank introns or span an intron-exon junction.
514 Amplicon range was 133-277 bp. All primers were tested on cDNA +/- reverse transcriptase and
515 gel electrophoresis to confirm the presence of a single product. Primer efficiencies were calculated
516 from 2-fold serial dilutions of cDNA. All primers are reported in Table S2.

517

518 For RNA extractions, 3 mm anteriors from 4-5 worms were cut, submerged in 200 µL TRIzol
519 Reagent (15596026; Invitrogen) and processed according to manufacturer's instructions with these
520 exceptions: 1) samples were homogenized with a motorized pestle twice in a semi-solid state then
521 centrifuged at >12K RCF for 5 min to obtain 180 µL clean supernatant, 2) RNA pellets were
522 washed twice with 75% ethanol-DEPC and 3); pellets were resuspended in 40 µL nuclease-free
523 water. DNAse (M6101; Promega) treatment was performed for 1 hr at 37°C. RNA was cleaned
524 using RNA Clean & Concentrator-5 kit (R1016; Zymo Research) and the concentration measured
525 on a Nanodrop spectrophotometer. cDNA synthesis was performed, according to manufacturer's
526 protocol, using Oligo$(dT)_{20}$ primers and iScript Select cDNA Synthesis Kit (1708897; Bio-Rad)
527 with undiluted RNA. cDNA was further diluted with 5-25 µL nuclease-free water depending on
528 the number of reactions needed.

529

530 qRT-PCR was performed using GoTaq MasterMix (A6001; Promega) according to manufacturer's
531 instructions and scaled to 25 µL reactions with 2 µL cDNA template for each of 3 technical
532 replicates. Each reaction had 0.4 µM primer pairs, 0.3 µM CXCR in 1X master mix. 7500 Real
533 Time PCR System (Applied Biosystems) was used for 40 amplification cycles: 15 s at 95°C and 1
534 min at 60°C. Relative gene expression change was calculated using the PFAFFL equation
535 (Hellemans et al., 2007; Vandesompele et al., 2002) to account for different primer efficiencies.
536 Internal normalization was done on the geometric mean of two previously published endogenous
537 controls: *60S ribosomal protein L13* (*60Srpl13;* WMSIL1_LOCUS3984) and *myosin heavy chain*
538 (*mhc;* WMSIL1_LOCUS8394) (Rozario et al., 2019) .

539

540 Statistical Analysis

541 Graph Pad Prism 10 was used for all statistical analyses. All experiments were repeated at least
542 twice. Error bars, statistical tests, number of replicates (N) and sample sizes (n) are indicated in
543 corresponding figure legends. P-values: ns= not significant, * = $p<0.05$, **=$p<0.01$, ***=$p<0.001$,
544 ****=$p<0.0001$.

Acknowledgements

We are sincerely thankful to Phil Newmark and Melanie Issigonis (Morgridge Institute for Research, WI). Phil's unwavering support in the initialization of these projects and continued advice was instrumental in our success. We are also grateful for Melanie's critical evaluation of our manuscript and valuable feedback. We thank the Biomedical Microscopy Core at the University of Georgia, Athens, GA for necessary microscopy services.

Competing interests

No conflicts to report.

Funding

This work was funded by a National Institute of Allergy and Infectious Disease (NIAID) grant (DP2 AI 154416-01) to Tania Rozario.

Data and resource availability

All relevant data and resources can be found within the article and its supplementary information.

561 **References**

562 **Aberle, H., Schwartz, H., Hoschuetzky, H. and Kemler, R.** (1996). Single Amino Acid
563 Substitutions in Proteins of the armadillo Gene Family Abolish Their Binding to α-Catenin*.
564 *J. Biol. Chem.* **271**, 1520–1526.

565 **Armstrong, R., Marks, N. J., Geary, T. G., Harrington, J., Selzer, P. M. and Maule, A. G.**
566 (2025). Wnt/β-catenin signalling underpins juvenile *Fasciola hepatica* growth and
567 development. *PLOS Pathog.* **21**, e1012562.

568 **Baguñà, J.** (2012). The planarian neoblast: the rambling history of its origin and some current
569 black boxes. *Int J Dev Biol.* **56**, 19–37.

570 **Bely, A. E. and Nyberg, K. G.** (2010). Evolution of animal regeneration: re-emergence of a
571 field. *Trends Ecol Evol.* **25**, 161–170.

572 **Blum, M., Chang, H.-Y., Chuguransky, S., Grego, T., Kandasaamy, S., Mitchell, A., Nuka,**
573 **G., Paysan-Lafosse, T., Qureshi, M., Raj, S., et al.** (2020). The InterPro protein families
574 and domains database: 20 years on. *Nucleic Acids Res.* **49**, D344–D354.

575 **Bolla, R. I. and Roberts, L. S.** (1971). Developmental physiology of cestodes. IX. Cytological
576 characteristics of the germinative region of *Hymenolepis diminuta*. *The Journal of*
577 *parasitology* **57**, 267–277.

578 **Bovolenta, P., Esteve, P., Ruiz, J. M., Cisneros, E. and Lopez-Rios, J.** (2008). Beyond Wnt
579 inhibition: new functions of secreted Frizzled-related proteins in development and disease. *J.*
580 *Cell Sci.* **121**, 737–746.

581 **Chai, G., Ma, C., Bao, K., Zheng, L., Wang, X., Sun, Z., Salò, E., Adell, T. and Wu, W.**
582 (2010). Complete functional segregation of planarian β-catenin-1 and -2 in mediating Wnt
583 signaling and cell adhesion. *The Journal of biological chemistry* **285**, 24120–24130.

584 **Collins, J. J., Hou, X., Romanova, E. V., Lambrus, B. G., Miller, C. M., Saberi, A.,**
585 **Sweedler, J. V. and Newmark, P. A.** (2010). Genome-wide analyses reveal a role for
586 peptide hormones in planarian germline development. *PLoS biology* **8**, e1000509.

587 **Collins, J. J., Wang, B., Lambrus, B. G., Tharp, M. E., Iyer, H. and Newmark, P. A.** (2013).
588 Adult somatic stem cells in the human parasite *Schistosoma mansoni*. *Nature* **494**, 476–479.

589 **Doddihal, V., Mann, F. G., Ross, E. J., McKinney, M. C., Guerrero-Hernández, C.,**
590 **Brewster, C. E., McKinney, S. A. and Alvarado, A. S.** (2024). A PAK family kinase and
591 the Hippo/Yorkie pathway modulate WNT signaling to functionally integrate body axes
592 during regeneration. *Proc. Natl. Acad. Sci.* **121**, e2321919121.

593 **Goodchild, C. G.** (1958). Transfaunation and Repair of Damage in the Rat Tapeworm,
594 *Hymenolepis diminuta*. *J. Parasitol* **44**, 345–351.

595 **Gurley, K. A., Rink, J. C. and Alvarado, A. S.** (2008). β-catenin defines head versus tail
596 identity during planarian regeneration and homeostasis. *Science* **319**, 323–327.

597 **Hellemans, J., Mortier, G., Paepe, A. D., Speleman, F. and Vandesompele, J.** (2007). qBase
598 relative quantification framework and software for management and automated analysis of
599 real-time quantitative PCR data. *Genome Biol.* **8**, R19.

600 **Herz, M., Zarowiecki, M., Wessels, L., Pätzel, K., Herrmann, R., Braun, C., Holroyd, N.,**
601 **Huckvale, T., Bergmann, M., Spiliotis, M., et al.** (2024). Genome-wide transcriptome
602 analysis of *Echinococcus multilocularis* larvae and germinative cell cultures reveals genes
603 involved in parasite stem cell function. *Front. Cell. Infect. Microbiol.* **14**, 1335946.

604 **Hill, E. M. and Petersen, C. P.** (2018). Positional information specifies the site of organ
605 regeneration and not tissue maintenance in planarians. *eLife* **7**, e02238.

606 **Holly, V. L., Widen, S. A., Famulski, J. K. and Waskiewicz, A. J.** (2014). Sfrp1a and Sfrp5
607 function as positive regulators of Wnt and BMP signaling during early retinal development.
608 *Dev. Biol.* **388**, 192–204.

609 **Iglesias, M., Gomez-Skarmeta, J. L., Saló, E. and Adell, T.** (2008). Silencing of *Smed-*
610 *βcatenin1* generates radial-like hypercephalized planarians. *Development* **135**, 1215–1221.

611 **Ishan, M., Skipper, I. R. and Rozario, T.** (2025). Combined fluorescent *in situ* hybridization
612 and F-ara-EdU staining on whole mount *Hymenolepis diminuta*. *Biol. Methods Protoc.*
613 bpaf011.

614 **Jarero, F., Baillie, A., Riddiford, N., Montagne, J., Koziol, U. and Olson, P. D.** (2024).
615 Muscular remodeling and anteroposterior patterning during tapeworm segmentation. *Dev.*
616 *Dyn.* **253**, 998–1023.

617 **Koziol, U., Rauschendorfer, T., Rodríguez, L. Z., Krohne, G. and Brehm, K.** (2014). The
618 unique stem cell system of the immortal larva of the human parasite *Echinococcus*
619 *multilocularis. EvoDevo* **5**, 10.

620 **Koziol, U., Jarero, F., Olson, P. D. and Brehm, K.** (2016). Comparative analysis of Wnt
621 expression identifies a highly conserved developmental transition in flatworms. *BMC biology*
622 **14**, 10.

623 **Laumer, C. E., Hejnol, A. and Giribet, G.** (2015). Nuclear genomic signals of the
624 "microturbellarian" roots of platyhelminth evolutionary innovation. *eLife* **4**, e05503.

625 **Leyns, L., Bouwmeester, T., Kim, S.-H., Piccolo, S. and Robertis, E. M. D.** (1997). Frzb-1 Is
626 a Secreted Antagonist of Wnt Signaling Expressed in the Spemann Organizer. *Cell* **88**, 747–
627 756.

628 **Liu, S. Y., Selck, C., Friedrich, B., Lutz, R., Vila-Farré, M., Dahl, A., Brandl, H.,**
629 **Lakshmanaperumal, N., Henry, I. and Rink, J. C.** (2013). Reactivating head regrowth in a
630 regeneration-deficient planarian species. *Nature* **500**, 81–84.

631 **Mii, Y. and Taira, M.** (2011). Secreted Wnt "inhibitors" are not just inhibitors: Regulation of
632 extracellular Wnt by secreted Frizzled-related proteins. *Dev., Growth Differ.* **53**, 911–923.

633 **Mohammed, M. K., Shao, C., Wang, J., Wei, Q., Wang, X., Collier, Z., Tang, S., Liu, H.,**
634 **Zhang, F., Huang, J., et al.** (2016). Wnt/β-catenin signaling plays an ever-expanding role in
635 stem cell self-renewal, tumorigenesis and cancer chemoresistance. *Genes Dis.* **3**, 11–40.

636 **Montagne, J., Preza, M., Castillo, E., Brehm, K. and Koziol, U.** (2019). Divergent Axin and
637 GSK-3 paralogs in the beta-catenin destruction complexes of tapeworms. *Dev. Genes. Evol.*
638 **11**, 1–14.

639 **Neef, A. B. and Luedtke, N. W.** (2011). Dynamic metabolic labeling of DNA in vivo with
640 arabinosyl nucleosides. *P.N.A.S.* **108**, 20404–20409.

641 **Nusse, R. and Clevers, H.** (2017). Wnt/β-Catenin Signaling, Disease, and Emerging
642 Therapeutic Modalities. *Cell* **169**, 985–999.

643 **Petersen, C. P. and Reddien, P. W.** (2008). *Smed-βcatenin-1* is required for anteroposterior
644 blastema polarity in planarian regeneration. *Science* **319**, 327–330.

645 **Petersen, C. P. and Reddien, P. W.** (2009). Wnt signaling and the polarity of the primary body
646 axis. *Cell* **139**, 1056–1068.

647 **Pokutta, S. and Weis, W. I.** (2000). Structure of the Dimerization and β-Catenin- Binding
648 Region of α-Catenin. *Mol. Cell* **5**, 533–543.

649 **Rattner, A., Hsieh, J.-C., Smallwood, P. M., Gilbert, D. J., Copeland, N. G., Jenkins, N. A.**
650 **and Nathans, J.** (1997). A family of secreted proteins contains homology to the cysteine-rich
651 ligand-binding domain of frizzled receptors. *Proc. Natl. Acad. Sci.* **94**, 2859–2863.

652 **Read, C. P.** (1967). Longevity of the tapeworm, *Hymenolepis diminuta*. *J Parasitol* **53**, 1055–6.

653 **Reddien, P. W.** (2018). The Cellular and Molecular Basis for Planarian Regeneration. *Cell* **175**,
654 327–345.

655 **Reuter, H., März, M., Vogg, M. C., Eccles, D., Grífol-Boldú, L., Wehner, D., Owlarn, S.,**
656 **Adell, T., Weidinger, G. and Bartscherer, K.** (2015). β-Catenin-Dependent Control of
657 Positional Information along the AP Body Axis in Planarians Involves a Teashirt Family
658 Member. *Cell Rep.* **10**, 253–265.

659 **Riddiford, N. and Olson, P. D.** (2011). Wnt gene loss in flatworms. *Dev. Genes. Evol.* **221**,
660 187–197.

661 **Roberts-Galbraith, R. H., Brubacher, J. L. and Newmark, P. A.** (2016). A functional
662 genomics screen in planarians reveals regulators of whole-brain regeneration. *eLife* **5**,
663 a000505.

664 **Rouhana, L., Weiss, J. A., Forsthoefel, D. J., Lee, H., King, R. S., Inoue, T., Shibata, N.,**
665 **Agata, K. and Newmark, P. A.** (2013). RNA interference by feeding in vitro-synthesized
666 double-stranded RNA to planarians: methodology and dynamics. *Dev. Dyn.* **242**, 718–730.

667 **Rozario, T. and Newmark, P. A.** (2015). A confocal microscopy-based atlas of tissue
668 architecture in the tapeworm *Hymenolepis diminuta*. *Exp. Parasitol.* **158**, 31–41.

669 **Rozario, T., Quinn, E. B., Wang, J., Davis, R. E. and Newmark, P. A.** (2019). Region-
670 specific regulation of stem cell-driven regeneration in tapeworms. *eLife* **8**, e48958.

671 **Schindelin, J., Arganda-Carreras, I., Frise, E., Kaynig, V., Longair, M., Pietzsch, T.,**
672 **Preibisch, S., Rueden, C., Saalfeld, S., Schmid, B., et al.** (2012). Fiji: an open-source
673 platform for biological-image analysis. *Nat. Methods* **9**, 676–682.

674 **Scimone, M. L., Cote, L. E., Rogers, T. and Reddien, P. W.** (2016). Two FGFRL-Wnt circuits
675 organize the planarian anteroposterior axis. *eLife* **5**, 905.

676 **Sikes, J. M. and Newmark, P. A.** (2013). Restoration of anterior regeneration in a planarian
677 with limited regenerative ability. *Nature* **500**, 77–80.

678 **Soria, C. L. D., Lee, J., Chong, T., Coghlan, A., Tracey, A., Young, M. D., Andrews, T.,**
679 **Hall, C., Ng, B. L., Rawlinson, K., et al.** (2020). Single-cell atlas of the first intra-
680 mammalian developmental stage of the human parasite *Schistosoma mansoni*. *Nat. Commun.*
681 **11**, 6411.

682 **Srivastava, M., Mazza-Curll, K. L., Wolfswinkel, J. C. van and Reddien, P. W.** (2014).
683 Whole-Body Acoel Regeneration Is Controlled by Wnt and Bmp-Admp Signaling. *Curr.*
684 *Biol.* **24**, 1107–1113.

685 **Steinhart, Z. and Angers, S.** (2018). Wnt signaling in development and tissue homeostasis.
686 *Development* **145**, dev146589.

687 **Stückemann, T., Cleland, J. P., Werner, S., Vu, H. T.-K., Bayersdorf, R., Liu, S.-Y.,**
688 **Friedrich, B., Jülicher, F. and Rink, J. C.** (2017). Antagonistic Self-Organizing Patterning
689 Systems Control Maintenance and Regeneration of the Anteroposterior Axis in Planarians.
690 *Dev. Cell* **40**, 248-263.e4.

691 **Su, H., Sureda-Gomez, M., Rabaneda-Lombarte, N., Gelabert, M., Xie, J., Wu, W. and**
692 **Adell, T.** (2017). A C-terminally truncated form of β-catenin acts as a novel regulator of
693 Wnt/β-catenin signaling in planarians. *PLoS Genet.* **13**, e1007030.

694 **Sureda-Gómez, M., Pascual-Carreras, E. and Adell, T.** (2015). Posterior Wnts Have Distinct
695 Roles in Specification and Patterning of the Planarian Posterior Region. *Int J Mol Sci.* **16**,
696 26543–26554.

697 **Tewari, A. G., Owen, J. H., Petersen, C. P., Wagner, D. E. and Reddien, P. W.** (2019). A
698 small set of conserved genes, including *sp5* and *Hox*, are activated by Wnt signaling in the
699 posterior of planarians and acoels. *PLoS Genet.* **15**, e1008401.

700 **Umesono, Y., Tasaki, J., Nishimura, Y., Hrouda, M., Kawaguchi, E., Yazawa, S.,**
701 **Nishimura, O., Hosoda, K., Inoue, T. and Agata, K.** (2013). The molecular logic for
702 planarian regeneration along the anterior-posterior axis. *Nature* **500**, 73–76.

703 **Üren, A., Reichsman, F., Anest, V., Taylor, W. G., Muraiso, K., Bottaro, D. P.,**
704 **Cumberledge, S. and Rubin, J. S.** (2000). Secreted Frizzled-related Protein-1 Binds Directly
705 to Wingless and Is a Biphasic Modulator of Wnt Signaling*. *J. Biol. Chem.* **275**, 4374–4382.

706 **Valenta, T., Hausmann, G. and Basler, K.** (2012). The many faces and functions of β-catenin.
707 *EMBO J.* **31**, 2714–2736.

708 **Vandesompele, J., Preter, K. D., Pattyn, F., Poppe, B., Roy, N. V., Paepe, A. D. and**
709 **Speleman, F.** (2002). Accurate normalization of real-time quantitative RT-PCR data by
710 geometric averaging of multiple internal control genes. *Genome Biol.* **3**, research0034.1.

711 **Wang, S., Krinks, M., Lin, K., Luyten, F. P. and Moos, M.** (1997). Frzb, a Secreted Protein
712 Expressed in the Spemann Organizer, Binds and Inhibits Wnt-8. *Cell* **88**, 757–766.

713 **Wang, B., Lee, J., Li, P., Saberi, A., Yang, H., Liu, C., Zhao, M. and Newmark, P. A.**
714 (2018). Stem cell heterogeneity drives the parasitic life cycle of *Schistosoma mansoni*. *eLife*
715 **7**, e35449.

716

717

718 **Figure legends**

719

720 **Fig. 1. The germinative region (GR) regenerates after amputation.** (A) Schematic of basic *H.*
721 *diminuta* anatomy and known regenerative ability. Head regeneration does not occur but
722 proglottids regenerate from fragments that retain the GR. Without the head region, proglottid
723 regeneration initially occurs but ceases. (B) DAPI-stained anterior fragments cut within the GR
724 (0.5 mm) or outside of it (2 mm) at 15 dpa. Quantification of worm length and proglottids
725 regenerated at 15 dpa. N= 3, n= 23, 27; t-test. (C) DAPI-stained 0.5 mm anterior regenerate at 15
726 dpa. Yellow arrowhead marks the first proglottid. Quantification of GR lengths from B; t-test. (D)
727 Quantification of proglottids regenerated every 2 days. Linear regression fitted; n= 50, 55. (E)
728 WISH for transcripts with A-P polarized expression patterns 3 days after acclimation *in vitro*
729 (uncut) then amputated at 0.5 mm and stained at 0 dpa and 10 dpa. Anterior toward the left.
730 Asterisks mark pigmented debris. Error bars= SD.

731

732 **Fig. 2. Serial amputation within the GR negatively affects regenerative ability.** (A) Scheme
733 for serial amputation within the GR. (B-C) Quantification of GR lengths and percentage of GR
734 length retained compared to GR lengths of uncut worms at 0 dpa per timepoint. Black squares=
735 means, gray circles= individual worms; N= 3, n= 29, 23; t-test. (D) Quantification of regeneration
736 success rate with F-test to compare variances (##: p=0.0015). (E) DAPI-stained regenerates 18
737 dpa. (F) Quantification of proglottids from worms that regenerated after cut 2. N= 3; n= 64, 25; t-
738 test. Error bars= SD.

739

740 **Fig. 3. The head inhibits proglottid regeneration and cell proliferation.** (A) DAPI-stained
741 regenerates from 0.5 mm amputations +/- head at 15 dpa. Quantification of proglottids regenerated
742 from a representative experiment. n= 7; t-test. (B) Confocal maximum intensity projections of +/-
743 head worms at 3 dpa immunostained for neuronal marker SYN after a 1 hr pulse of F-*ara*-EdU to
744 label proliferating cells. Quantification of proliferation density within the GR from a representative
745 experiment. Each sample was normalized to the mean proliferation density in the corresponding
746 +head group. n= 10, 12; t-test. (C-D) Confocal maximum intensity projections after 1 hr pulse of
747 F-*ara*-EdU +/- head at 3 dpa. Yellow dotted lines represent 200 μm-wide regions used for

748 quantification of proliferation density. H= head. N= 3, n= 11, 13; one-way ANOVA with Dunnett's
749 multiple comparison test. Error bars= SD.
750
751 **Fig. 4. Effect of head or head-adjacent amputations on proliferation and regeneration.** (A)
752 Scheme for results shown in B-C and Fig. S3. Step 1: Four amputation schemes tested: intact head
753 (+head), transverse cut through half the head while retaining the brain (½ head), head removal (-
754 head) and cut 0.5 mm from the anterior into the GR (-0.5 mm). Step 2: all worms were amputated
755 posteriorly to obtain 2 mm fragments. Step 3: fragments were grown *in vitro* for 14 days. Step 4-
756 5: regenerates were recut to obtain 2 mm anterior fragments that were cultured *in vitro* while the
757 posteriors were collected to measure proglottid regeneration. (B) Quantification of proglottids
758 regenerated. All samples were normalized to the mean of +head worms set to 100%. Bars indicate
759 means for all samples after cut 1 and only for samples with visible GRs for cut 2-4. Proglottidized
760 worms without GRs= red dots, n= 27, 37, 26, 19 by scheme at start. (C) Percentage of regenerates
761 that maintained a visible GR from B. (D) After cut 4, proglottids regenerated from +head and ½
762 head samples from one experiment plotted against head area remaining measured from DAPI-
763 stained worms. Linear regression fitted; n= 8, 12. (E-F) Quantification of F-*ara*-EdU+ cells
764 normalized to GR area at 3 dpa. All samples were normalized to the mean of +head worms set to
765 100%. N= 4, 3, 4, 3 by scheme; two-way ANOVA (mixed model) and Tukey's multiple
766 comparison test (E). All pooled data from E analyzed with one-way ANOVA compared to +head
767 with Dunnett's multiple comparison test; n= 26, 28, 26, 21 by scheme. Error bars= SD.
768
769 **Fig. 5. *βcat1* is a posterior-biased factor that is necessary to maintain the cycling stem cell**
770 **population in the GR.** (A) Schematic and WISH of *βcat1* expression at the GR from 6-day-old
771 adult. (B) RNAi scheme and DAPI-stained worms at 7 dpa. (C) Quantification of worm lengths
772 after RNAi at 7 dpa. Bars= means, gray circles= individual worms; N= 3, n= 24, 24, 23; one-way
773 ANOVA with Dunnett's multiple comparison test. (D) qRT-PCR for target gene expression (top)
774 after *βcat1* RNAi compared to *GFP* RNAi (set at 1). (E) Representative maximum intensity
775 confocal projections at the GR after 1 hr F-*ara*-EdU uptake. Dotted yellow lines= worm outlines.
776 Quantification of F-*ara*-EdU+ cells normalized to area from 800 µm-wide cropped region
777 posterior to the head at 6-7 dpi. All samples were normalized to the mean of *GFP* RNAi worms
778 set to 100%. Bars= means, gray circles= individual worms; N= 3, n= 20, 19, 16; one-way ANOVA

779 with Dunnett's multiple comparison test. (F) WISH for cycling stem cell markers *mcm2* and *lbr* at
780 6 dpi; N= 3. Error bars= SD.
781
782 **Fig. 6. *sfrp* is an anterior-biased factor that regulates GR length.** (A) Schematic and WISH of
783 *sfrp* expression at the GR from 6-day-old adult. (B) RNAi scheme for C-F. (C) Representative
784 DAPI-stained regenerates after RNAi. (D) Quantification of proglottids regenerated after RNAi
785 normalized to mean from *GFP* RNAi set to 100%. (E) Representative DAPI-stained images
786 showing GR lengths (between yellow arrowheads). (F) Quantification of GR lengths from D. For
787 D, F: Bars= means, gray circles= individual worms; N= 3, n = 26, 25, 25; one-way ANOVA with
788 Dunnett's multiple comparison test; error bars= SD.
789
790 **Fig. 7. How amputations at increasing distance from the head influence competence to**
791 **regenerate.** (A) Regenerates from 0.5 mm anterior fragments grown for 18 days were re-
792 amputated at 1 mm (cut A). A subset was fixed to quantify GR length and a subset was grown *in*
793 *vitro* for 18 days. The remaining fragments were recut to shave off ~20-25% GR (cut B) and the
794 process repeated successively for cut C and cut D. Darkfield images showing live fragments before
795 *in vitro* culture. (B) GR lengths measured from DAPI-stained 0 dpa fragments represented as
796 percentage of GR length relative to uncut worms from the same cohort. N=3, n= 20, 21, 21, 21;
797 two-way ANOVA (mixed model) with Tukey's multiple comparison test. (C) Percentage of
798 fragments that regenerated proglottids after 18 days. N= 3, n= 27, 23, 21, 22 at start. Each
799 experiment is represented by the same color in B and C. Colored arrows point to matched sets
800 representing groups with lowest regeneration success. (D-F) Quantification of worm length (D),
801 growth fold change (E) and GR length (F). N= 3, n= 20, 8, 10, 17; t-test. Error bars= SD.
802
803 **Fig. 8. Working model for regeneration in *H. diminuta*.** Overlapping regions at the head (blue
804 bars) play two contrasting roles: proliferation and proglottidization rate are negatively regulated
805 whereas GR maintenance is positively regulated. *βcat1* expression is posteriorly biased and *βcat1*
806 is necessary to maintain stem cells in the GR, which are required for proglottid regeneration.
807 Expression of *sfrp* is anteriorly biased and *sfrp* is necessary to maintain GR length. Signals that
808 may link the head/brain/anterior GR to *βcat1* and *sfrp* expression or activity remain to be
809 identified. Serial amputation within the GR revealed increased failure to regenerate the GR and

810 proglottids (yellow X) at intermediate distances forming a tipping point zone that is refractory to
811 regeneration (black shading). Both smaller and larger fragments amputated outside of the black
812 region regenerated equivalently (green check).
813
814 **Fig. S1. Specificity of antisense riboprobes.** WISH with antisense and sense riboprobes for
815 transcripts in Fig. 1E.
816
817 **Fig. S2. Proliferation response at wound site.** Worms were amputated at 0.5 mm within the GR.
818 Proliferation density was quantified from a 100 μm-wide box at the posterior-facing wound (Pfw)
819 and anterior-facing wound (Afw) at 1 dpa after 1 hr pulse of F-*ara*-EdU. Quantification from one
820 representative experiment, n= 6, 5, 6, 7; error bars= SD, one-way ANOVA with Tukey's multiple
821 comparison test.
822
823 **Fig. S3. How head tissues influence regeneration.** (A) Widefield fluorescent images of ½ head
824 fragments at 0 dpa stained with anti-SYN antibodies. Yellow arrowheads point to the
825 brain/cephalic ganglia. (B) GR lengths at the end of a representative serial amputation experiment.
826 n= 5, 8, 8; one-way ANOVA with Dunnett's multiple comparison test. (C) Quantification of
827 proglottids regenerated after cut 1, normalized to +head means. N= 3; n= 27, 37, 26; statistical
828 significance by one-way ANOVA and was the same for all 3 experiments. (D) Quantification of
829 proglottids regenerated normalized to +head means. Cut 2: N= 3, n= 27, 34; Cut 3: N= 2, n= 11,
830 16; Cut 4: N= 2, n= 13, 15; t-tests. Error bars= SD.
831
832 **Fig. S4. Domain analysis of *H. diminuta* βCAT1.** (A) Sequence alignment of βCAT1 from four
833 flatworms (*Hd: H. diminuta, Em: E. multilocularis, Sm: S. mansoni, Smed: S. mediterranea*). The
834 conserved DSGxxSxxx[S/T]xxxS motif for CKI/GSK-phosphorylation (red) is present as are
835 armadillo repeats (lilac). The boundaries of both domains are shown according to *S. mediterranea*
836 (Su et al., 2017). Shading indicates identical residues between 4 species (gray) or 3 species (blue).
837 The N- and C-termini are more divergent between all species. (B) Sequence alignment of 26 amino
838 acids covering a putative α-catenin binding domain (Montagne et al., 2019). 10 critical residues
839 for α-catenin binding (Aberle et al., 1996; Pokutta and Weis, 2000) are marked by α (green). In
840 reference to human CTNB1, dark gray shading highlights identical residues. Chemically similar

841 residues marked in light gray for aromatic (F, Y, W, H), aliphatic (V, I, L), positively charged (R,
842 K, H), negatively charged (D, E), polar but not charged (N, Q, T, S, Y, C) and hydrophobic (V, I,
843 L, M, A, F, P, W, G) residues.
844
845 **Fig. S5. WISH for *βcat1, axin1, axin2* and *sfrp*.** Representative micrographs spanning different
846 stages of development in 6-day-old worms with anterior facing left.
847
848 **Fig. S6. Domain analysis of *H. diminuta* SFRP.** BLASTp alignment of SFRPs from flatworms
849 and human SFRP-1,-2 and -5 as references (*Hd: H. diminuta, Em: E. multilocularis, Smed: S.*
850 *mediterranea*). The frizzled domain (orange) and netrin domain (blue) are marked at the most
851 inclusive positions reported for human SFRP1 using Interpro (Blum et al., 2020). Conserved
852 cysteines highlighted in yellow.
853
854 **Fig. S7. Phenotypes observed after *sfrp* RNAi and head amputation.** (A) Scheme for RNAi
855 with dsRNA injections throughout the GR. (B-C) Quantification of proglottid regeneration (B) and
856 GR length (C) from two independent experiments; Exp 1: n= 8, 8, 9, Exp 2: n= 8, 8, 7; one-way
857 ANOVA with Dunnett's multiple comparison test. (D) qRT-PCR following dsRNA injection at
858 the head/scolex (Sc-biased) or throughout the GR. Expression of *sfrp* (target) after *sfrp* RNAi
859 compared to *GFP* RNAi (set at 1); t-test. (E) qRT-PCR for *sfrp* expression compared to +head (set
860 at 1); t-test. (F) WISH for *sfrp* at representative worm anteriors from +/- head worms 3 dpa.
861 Anterior facing left. (D) Quantification of F-*ara*-EdU+ cells normalized to area from 800 µm-wide
862 cropped region posterior to the head or to the first proglottid. Combined from single and double
863 dsRNA injections throughout the GR with significant *sfrp* knockdown. All samples were
864 normalized to the mean of *GFP* RNAi worms set to 100%. Bars= means, gray circles= individual
865 worms; N= 3, n= 22, 21, 23; one-way ANOVA with Dunnett's multiple comparison test. Error
866 bars= SD.
867
868 **Fig. S8. Comparison of regenerates from longest vs. shortest fragment groups after re-**
869 **amputation.** (A) DAPI-stained regenerates at 18 dpa. (B) Proglottid regeneration at 18 dpa. N= 3,
870 n= 20, 17; t-test; error bars= SD.
871

872 **Table S1. *βcatenin* paralogs in *H. diminuta.***

873

874 **Table S2. Primers and transcripts used in this study.**

875

876 **Table S3. Source data used in this study.**

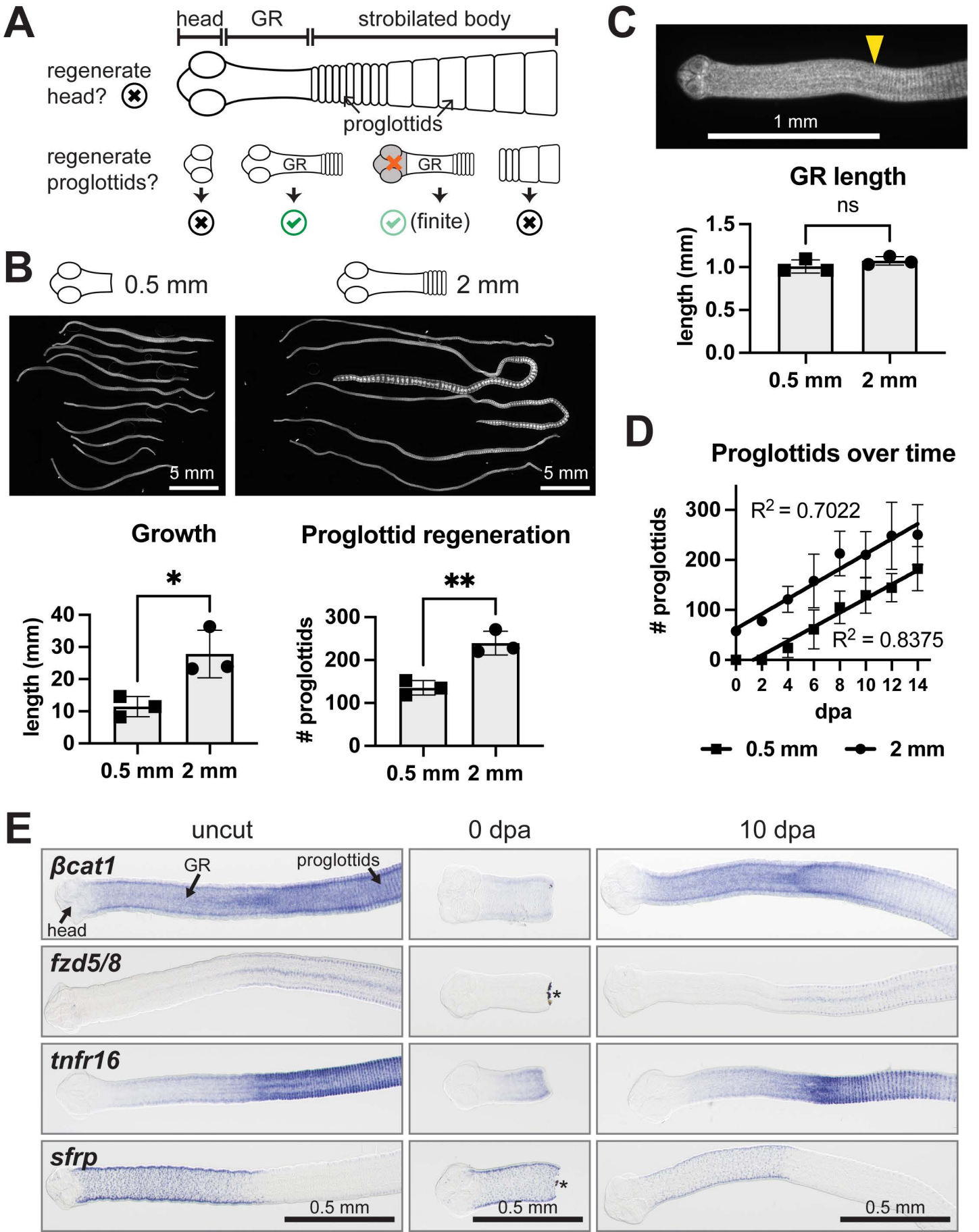
A
head
GR
strobilated body
regenerate head?
proglottids
regenerate proglottids?
GR
GR
(finite)
B
0.5 mm
2 mm
5 mm
5 mm
Growth
*
length (mm)
40
30
20
10
0
0.5 mm
2 mm
Proglottid regeneration
**
proglottids
300
200
100
0
0.5 mm
2 mm
C
1 mm
GR length
ns
length (mm)
1.5
1.0
0.5
0.0
0.5 mm
2 mm
D
Proglottids over time
proglottids
300
200
100
0
R2 = 0.7022
R2 = 0.8375
0
2
4
6
8
10
12
14
dpa
0.5 mm
2 mm
E
uncut
0 dpa
10 dpa
βcat1
GR
proglottids
head
fzd5/8
tnfr16
sfrp
0.5 mm
0.5 mm
0.5 mm

Figure 2

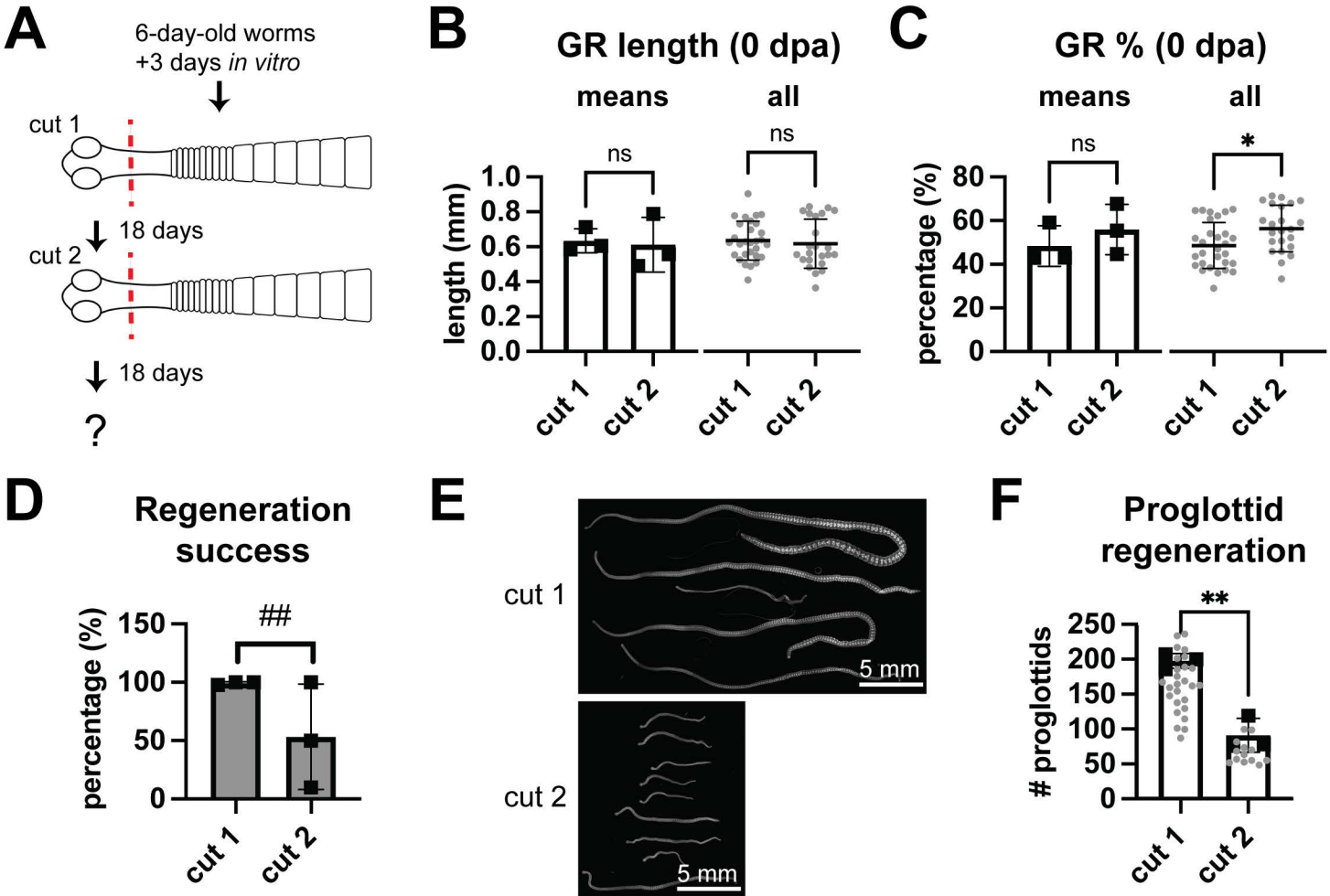
A
6-day-old worms
+3 days in vitro
cut 1
18 days
cut 2
18 days
?
B
GR length (0 dpa)
means
all
ns
ns
length (mm)
1.0
0.8
0.6
0.4
0.2
0.0
cut 1
cut 2
cut 1
cut 2
C
GR % (0 dpa)
means
all
ns
*
percentage (%)
80
60
40
20
0
cut 1
cut 2
cut 1
cut 2
D
Regeneration success
##
percentage (%)
150
100
50
0
cut 1
cut 2
E
cut 1
5 mm
cut 2
5 mm
F
Proglottid regeneration
**
proglottids
250
200
150
100
50
0
cut 1
cut 2

Figure 3

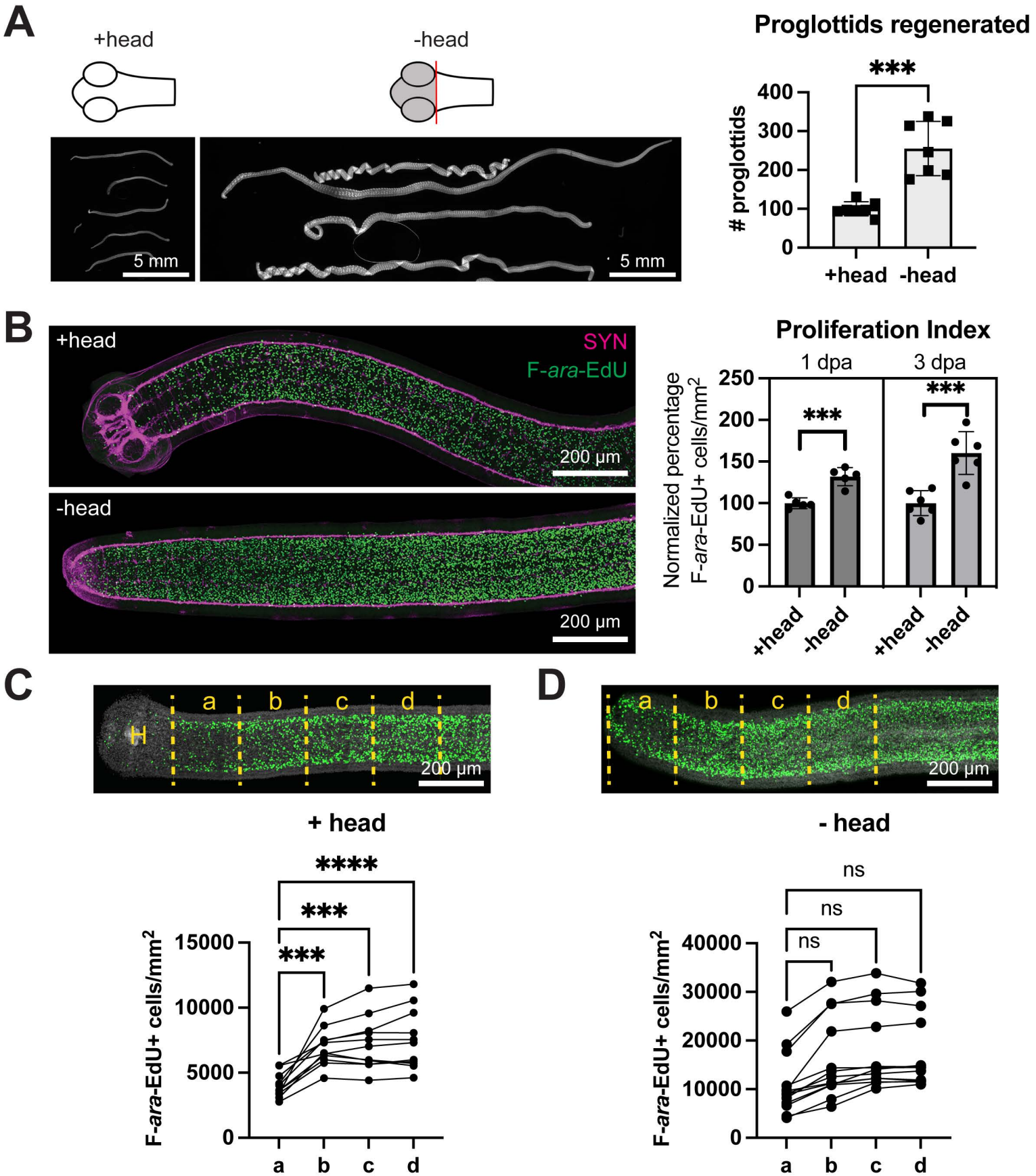
A
+head
-head
5 mm
5 mm
Proglottids regenerated
***
proglottids
400
300
200
100
0
+head
-head
B
+head
SYN
F-ara-EdU
200 µm
-head
200 µm
Proliferation Index
1 dpa
3 dpa
Normalized percentage F-ara-EdU+ cells/mm2
250
200
150
100
50
0
***
***
+head
-head
+head
-head
C
a
b
c
d
H
200 µm
+ head
****
***
***
F-ara-EdU+ cells/mm2
15000
10000
5000
0
a
b
c
d
D
a
b
c
d
200 µm
- head
ns
ns
ns
F-ara-EdU+ cells/mm2
40000
30000
20000
10000
0
a
b
c
d

Figure 4

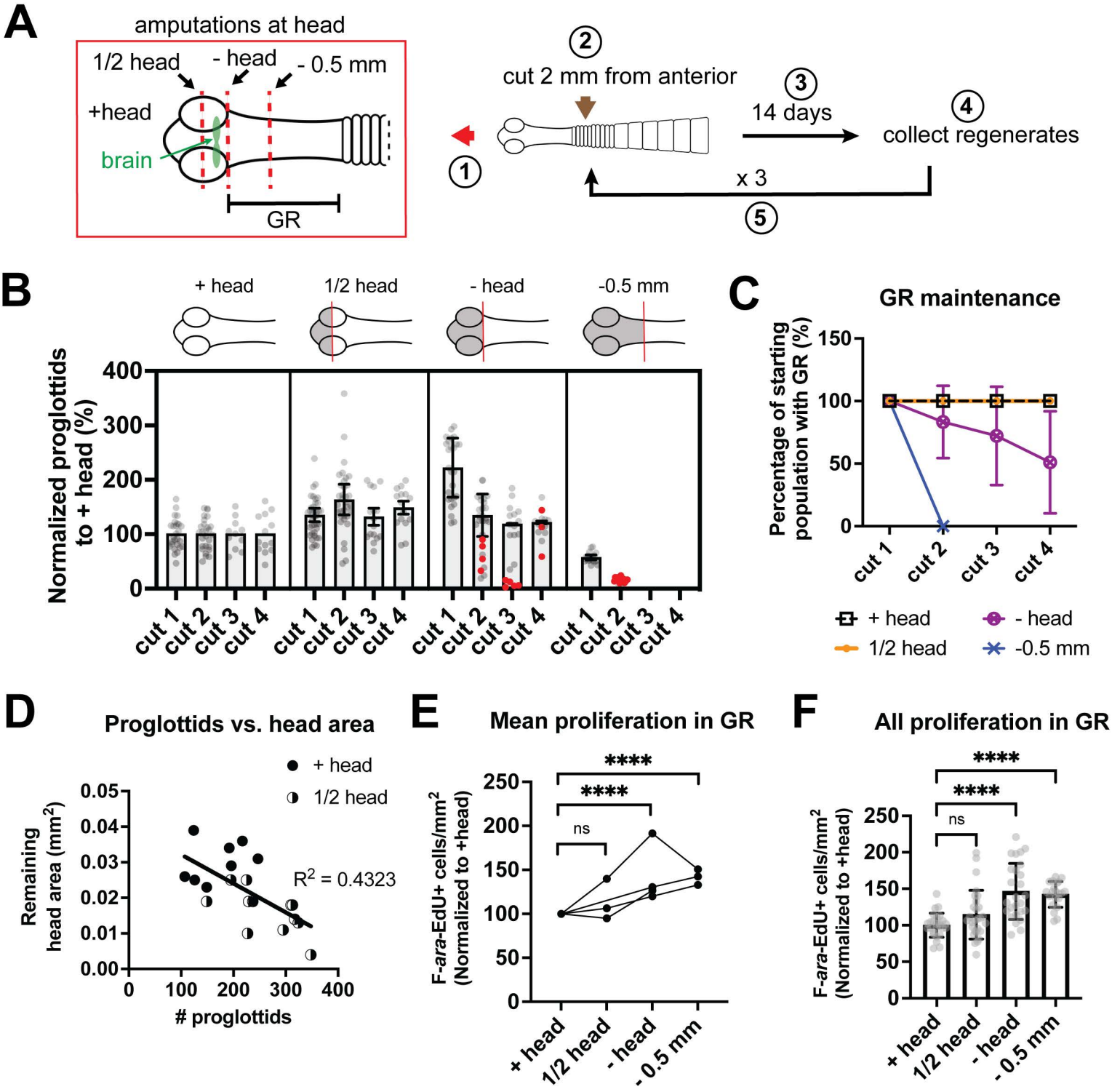
A
amputations at head
1/2 head
- head
- 0.5 mm
+head
brain
GR
1
2
cut 2 mm from anterior
3
14 days
4
collect regenerates
x 3
5
B
+ head
1/2 head
- head
-0.5 mm
Normalized proglottids to + head (%)
400
300
200
100
0
cut 1
cut 2
cut 3
cut 4
C
GR maintenance
Percentage of starting population with GR (%)
150
100
50
0
cut 1
cut 2
cut 3
cut 4
+ head
- head
1/2 head
-0.5 mm
D
Proglottids vs. head area
+ head
1/2 head
Remaining head area (mm²)
0.05
0.04
0.03
0.02
0.01
0.00
R² = 0.4323
0
100
200
300
400
proglottids
E
Mean proliferation in GR
F-ara-EdU+ cells/mm² (Normalized to +head)
250
200
150
100
50
0
****
****
ns
+ head
1/2 head
- head
- 0.5 mm
F
All proliferation in GR
F-ara-EdU+ cells/mm² (Normalized to +head)
250
200
150
100
50
0
****
****
ns
+ head
1/2 head
- head
- 0.5 mm

Figure 5

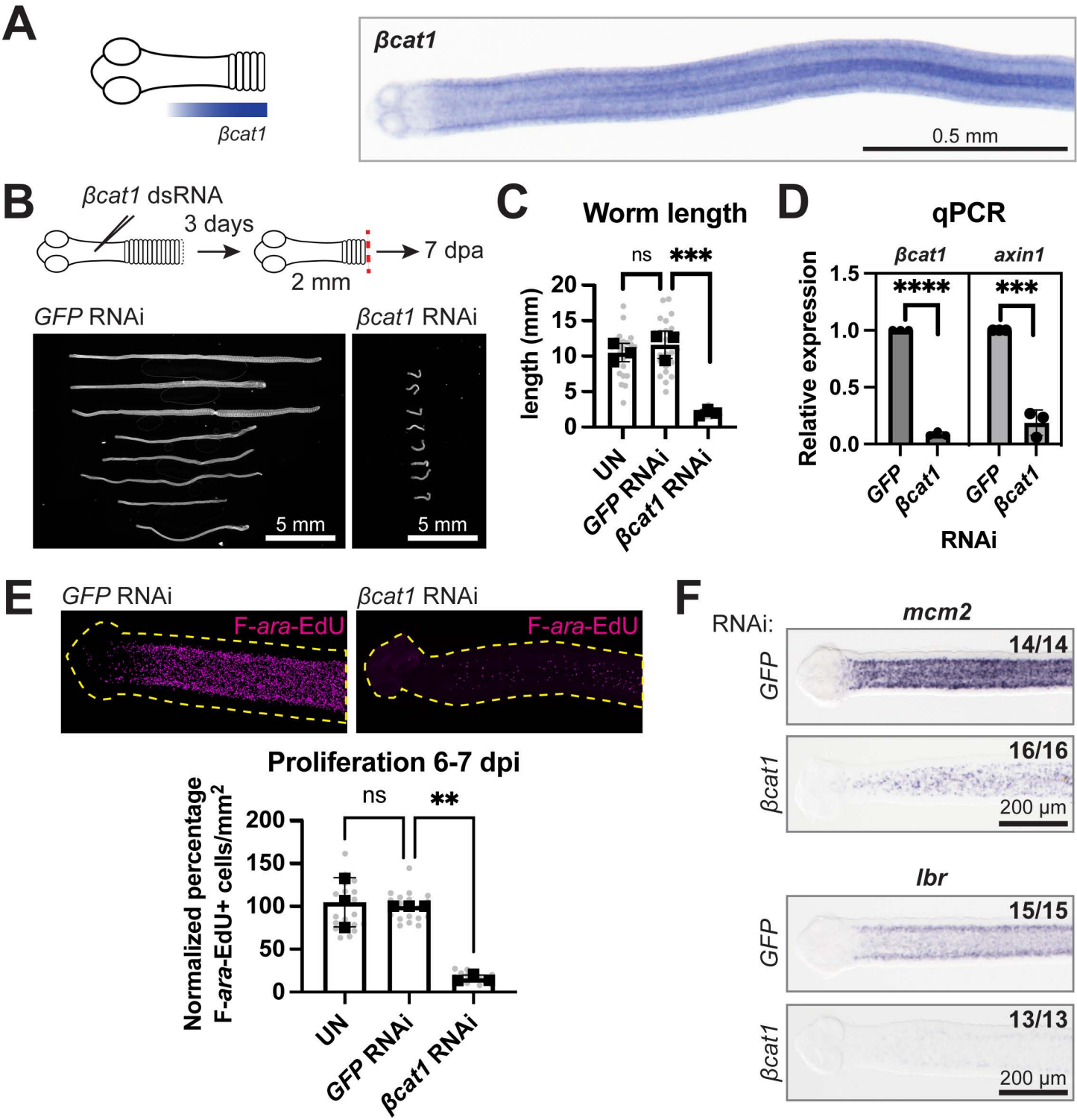
A
βcat1
βcat1
0.5 mm
B
βcat1 dsRNA
3 days
2 mm
7 dpa
GFP RNAi
βcat1 RNAi
5 mm
5 mm
C
Worm length
ns
***
length (mm)
20
15
10
5
0
UN
GFP RNAi
βcat1 RNAi
D
qPCR
βcat1
axin1
****
***
Relative expression
1.5
1.0
0.5
0.0
GFP
βcat1
GFP
βcat1
RNAi
E
GFP RNAi
βcat1 RNAi
F-ara-EdU
F-ara-EdU
Proliferation 6-7 dpi
ns
**
Normalized percentage F-ara-EdU+ cells/mm2
200
150
100
50
0
UN
GFP RNAi
βcat1 RNAi
F
RNAi:
mcm2
GFP
14/14
βcat1
16/16
200 µm
lbr
GFP
15/15
βcat1
13/13
200 µm

Figure 6

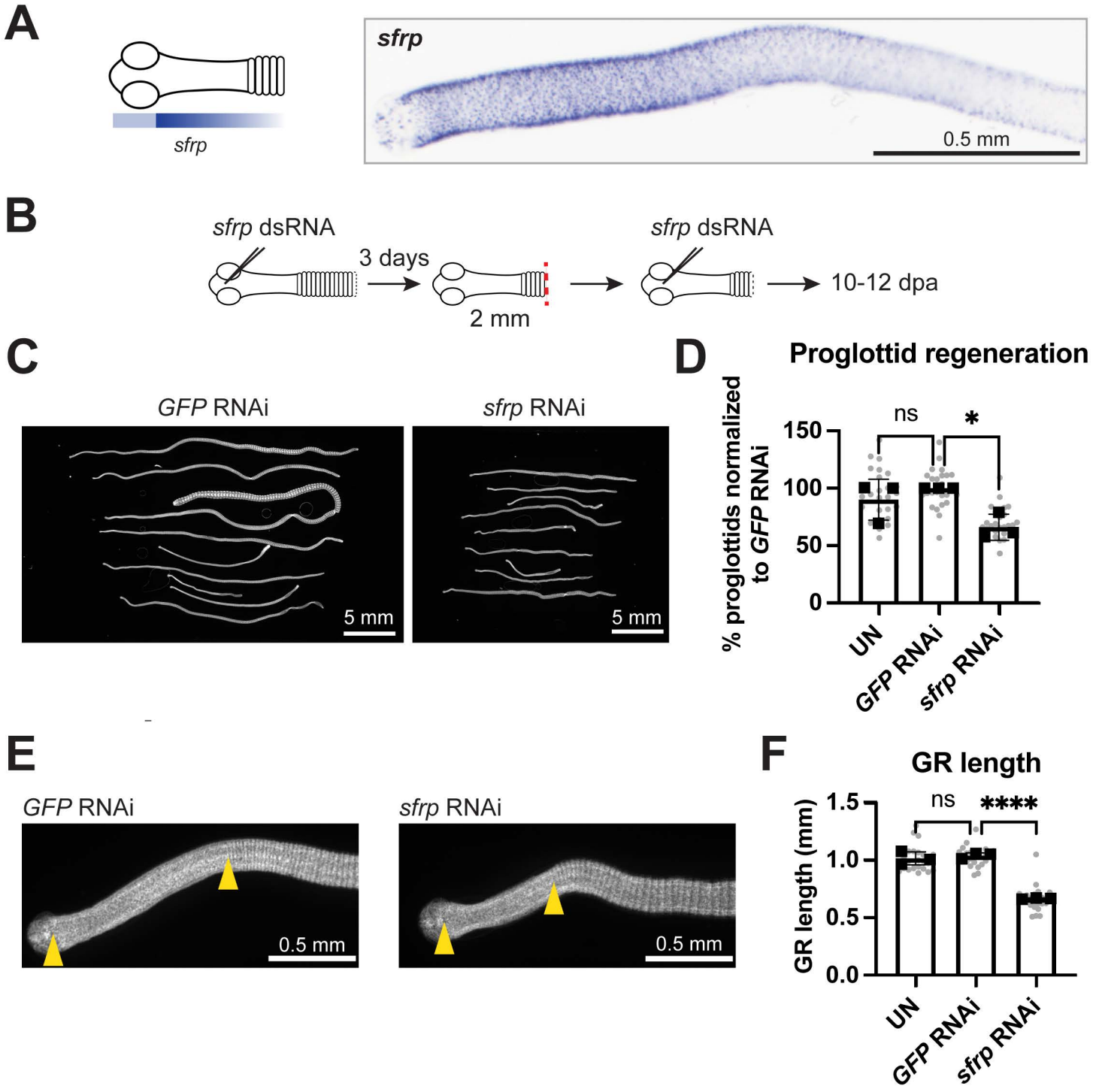
A
sfrp
sfrp
0.5 mm
B
sfrp dsRNA
3 days
2 mm
sfrp dsRNA
10-12 dpa
C
GFP RNAi
sfrp RNAi
5 mm
5 mm
D
Proglottid regeneration
% proglottids normalized to GFP RNAi
150
100
50
0
ns
*
UN
GFP RNAi
sfrp RNAi
E
GFP RNAi
sfrp RNAi
0.5 mm
0.5 mm
F
GR length
GR length (mm)
1.5
1.0
0.5
0.0
ns
****
UN
GFP RNAi
sfrp RNAi

Figure 7

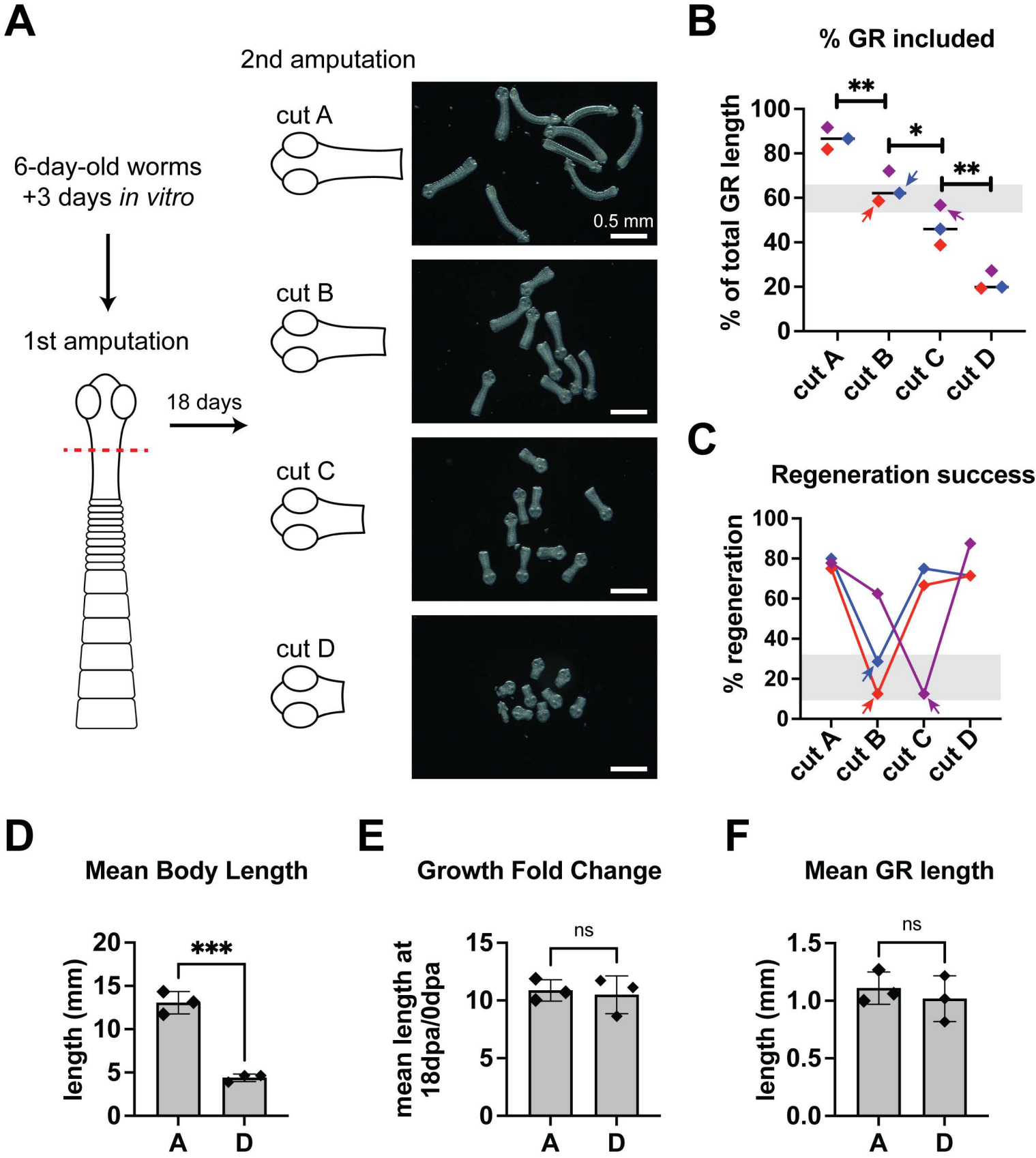
A
2nd amputation
6-day-old worms
+3 days in vitro
1st amputation
18 days
cut A
cut B
cut C
cut D
0.5 mm
B
% GR included
% of total GR length
100
80
60
40
20
0
**
*
**
cut A
cut B
cut C
cut D
C
Regeneration success
% regeneration
100
80
60
40
20
0
cut A
cut B
cut C
cut D
D
Mean Body Length
length (mm)
20
15
10
5
0
***
A
D
E
Growth Fold Change
mean length at 18dpa/0dpa
15
10
5
0
ns
A
D
F
Mean GR length
length (mm)
1.5
1.0
0.5
0.0
ns
A
D

Figure 8

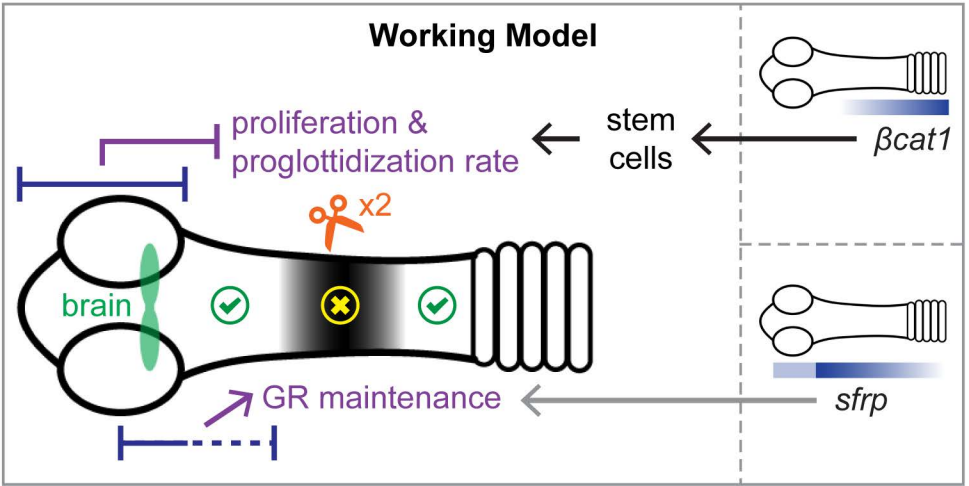
Working Model
proliferation &
proglottidization rate
stem
cells
βcat1
x2
brain
GR maintenance
sfrp

Figure S1

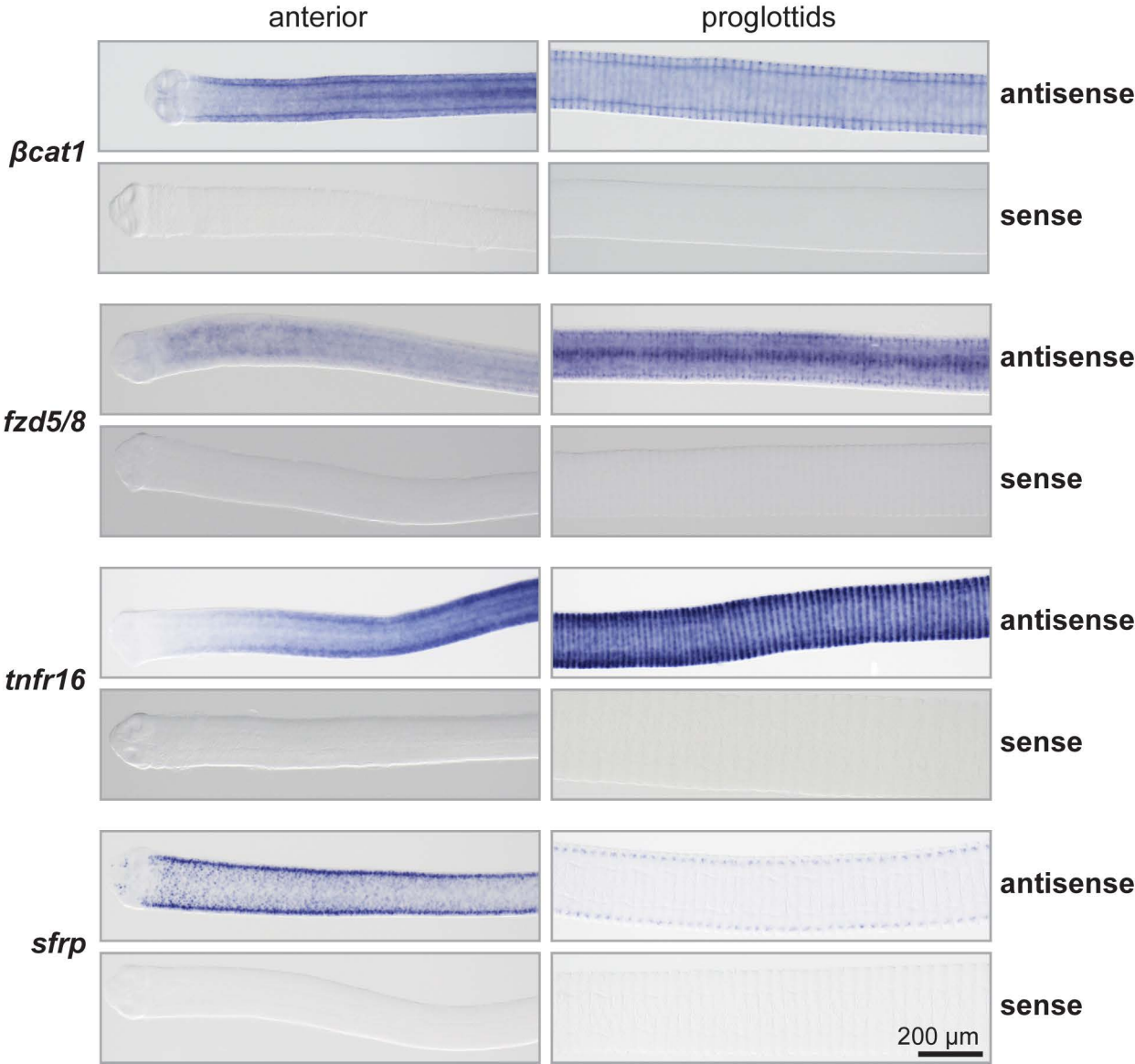
anterior
proglottids
βcat1
antisense
sense
fzd5/8
antisense
sense
tnfr16
antisense
sense
sfrp
antisense
sense
200 µm

Figure S2

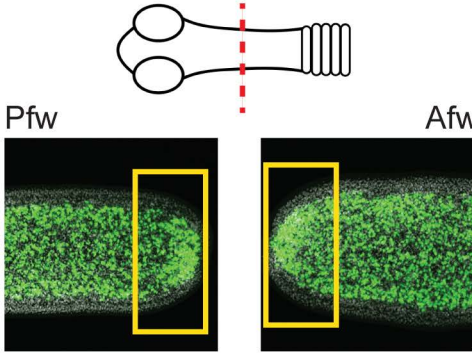
Pfw
Afw

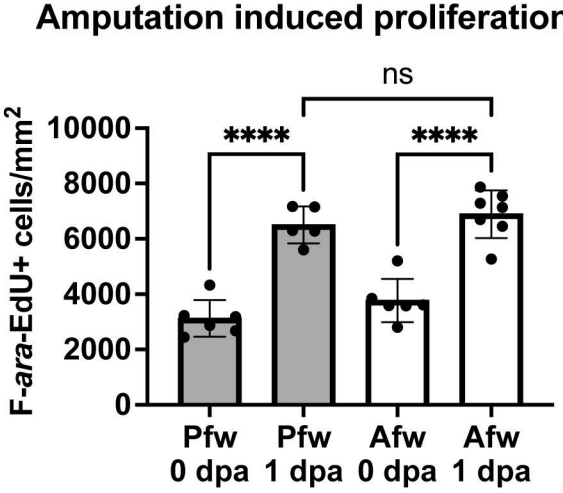
Amputation induced proliferation
ns
****
****
F-ara-EdU+ cells/mm2
10000
8000
6000
4000
2000
0
Pfw 0 dpa
Pfw 1 dpa
Afw 0 dpa
Afw 1 dpa

Figure S3

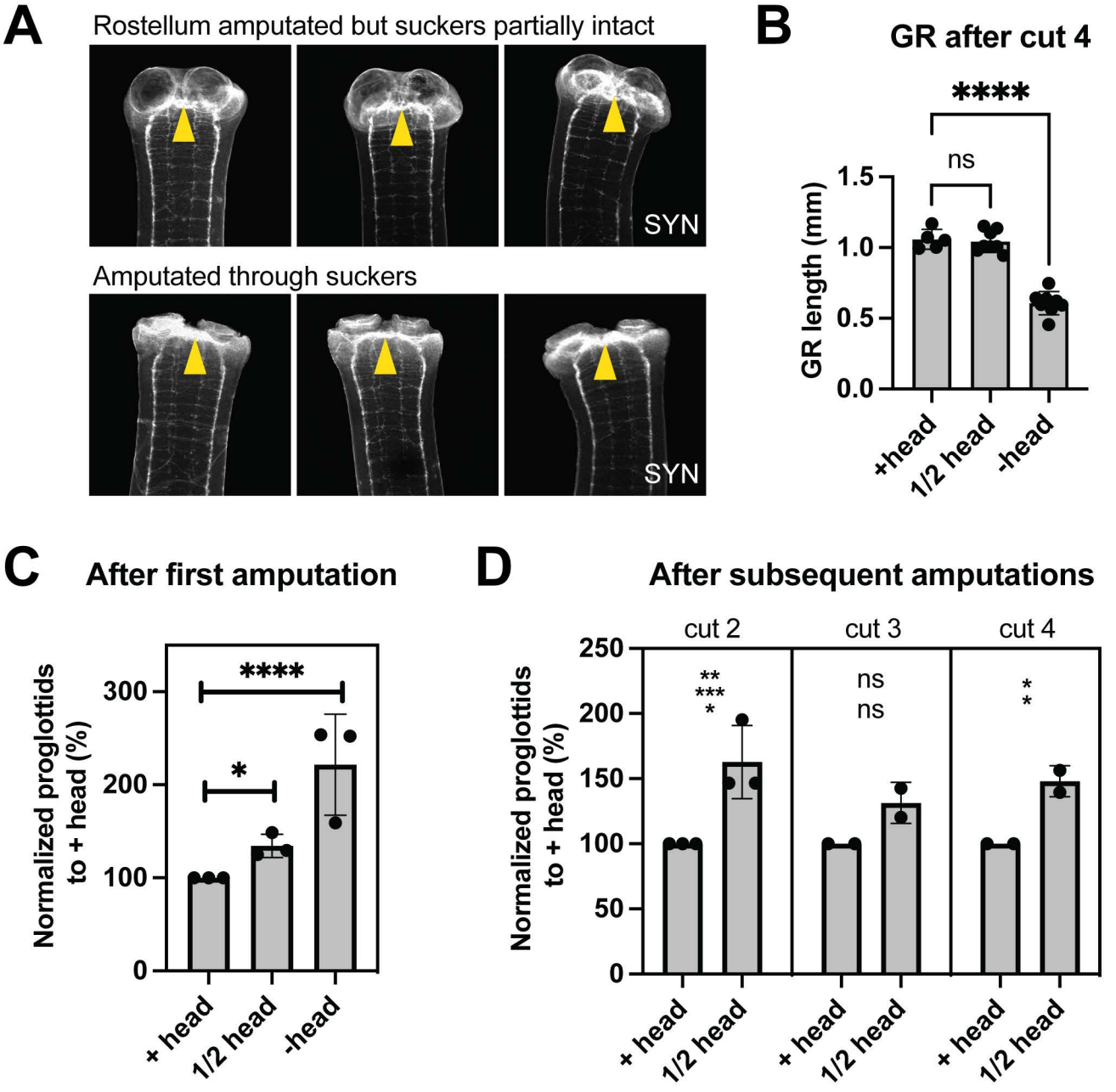
A
Rostellum amputated but suckers partially intact
SYN
Amputated through suckers
SYN
B
GR after cut 4
****
ns
GR length (mm)
1.5
1.0
0.5
0.0
+head
1/2 head
-head
C
After first amputation
****
*
Normalized proglottids to + head (%)
300
200
100
0
+ head
1/2 head
-head
D
After subsequent amputations
cut 2
cut 3
cut 4
**
***
*
ns
ns
*
*
Normalized proglottids to + head (%)
250
200
150
100
50
0
+ head
1/2 head
+ head
1/2 head
+ head
1/2 head

Figure S4

A

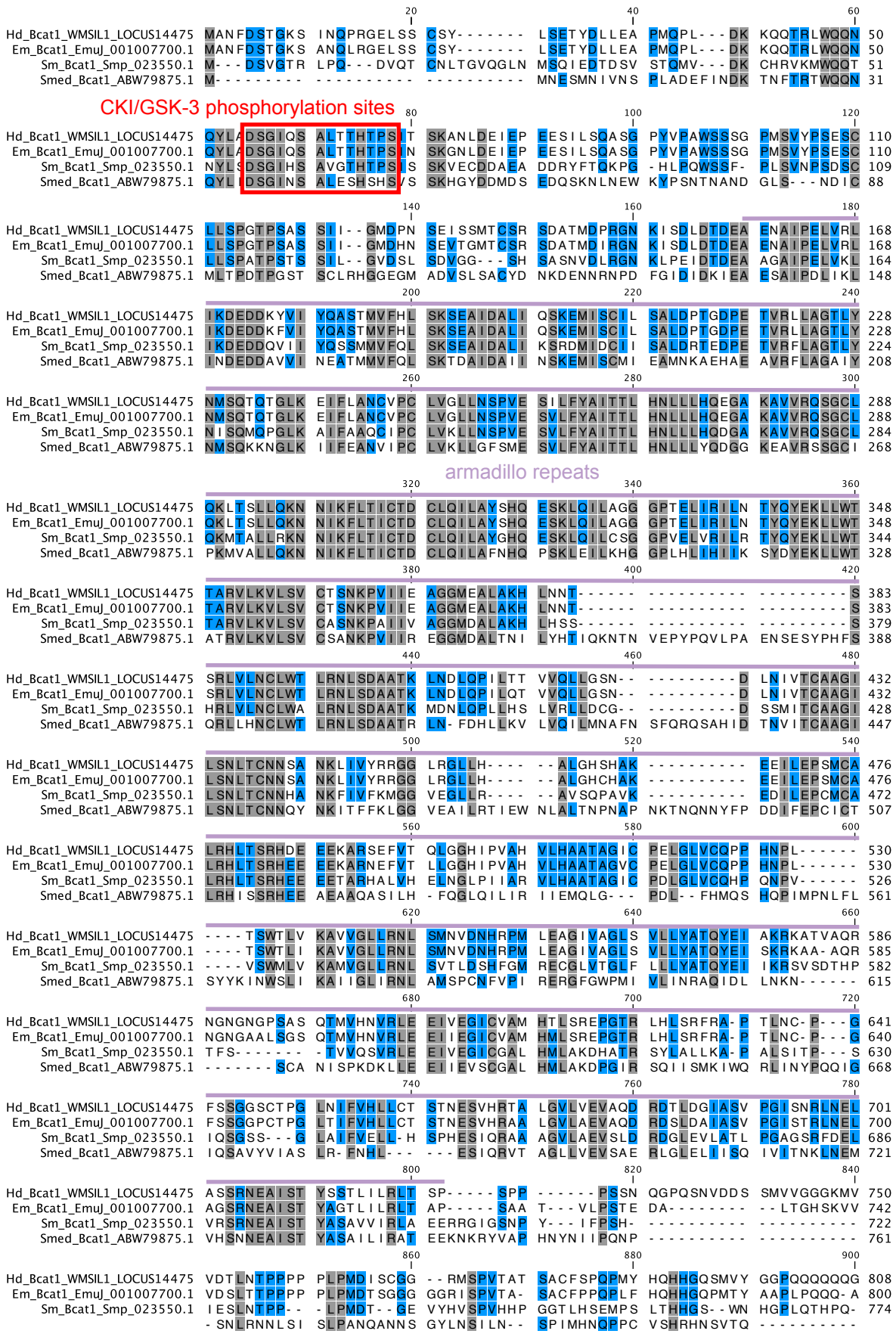
CKI/GSK-3 phosphorylation sites
armadillo repeats
Hd_Bcat1_WMSIL1_LOCUS14475
Em_Bcat1_EmuJ_001007700.1
Sm_Bcat1_Smp_023550.1
Smed_Bcat1_ABW79875.1

```
                                                  920                                 940                                 960
                                                   |                                   |                                   |
Hd_Bcat1_WMSIL1_LOCUS14475  PPLQRYAPPP  PGSYHYSNNE  PVGSGGNGGG  ----SLMAMV  GPPPNSSAYS  GGNS-----G  859
 Em_Bcat1_EmuJ_001007700.1  PSVQRYAP--  -GGYHYSGEA  VAGPGGGGGG  GSGGSLMAMV  GPPPPASVYS  VSGS-----G  852
     Sm_Bcat1_Smp_023550.1  ----------  ----------  ---ESGNTCG  SPSNSLMEML  GPFPPGCKGS  VCNDCCSYWG  811
     Smed_Bcat1_ABW79875.1  ----------  ----------  --------CG  DQNIATNETL  ----------  ----------  820
                                                  980                                1,000                               1,020
                                                   |                                   |                                   |
Hd_Bcat1_WMSIL1_LOCUS14475  GCPMNVQQQM  PPQQ-HPPHC  YQQQPMNENA  YQQCSWGNPS  YPQEPQGRPV  YANQMPPHHA  918
 Em_Bcat1_EmuJ_001007700.1  PCPMSVQS-M  PPQQ-HP-HC  YQQQPMNEAA  YPQRSWGNGP  YASDPQGRPL  YANTMAPHHP  909
     Sm_Bcat1_Smp_023550.1  DCD-------  PPGTCSDPNC  IYNG------  --NNSQSSGT  Y-SELQPVKL  YHNI------  849
     Smed_Bcat1_ABW79875.1  -CPIN---DV  DVTDYHMPFS  NTLQPQNR--  ----------  YPYNP-----  --NFVDPNYS  857
                                                 1,040                               1,060                               1,080
                                                   |                                   |                                   |
Hd_Bcat1_WMSIL1_LOCUS14475  PPAQQPQSQE  GMYGPPGMGY  IQP---SGNM  RGVQPAYHHR  SSPAAAQGGY  Y---------  966
 Em_Bcat1_EmuJ_001007700.1  PPAQQ--QQE  TLYGPPGMGY  PPP---SGSV  RDMPPAYHHR  GSPAAA--GY  Y---------  953
     Sm_Bcat1_Smp_023550.1  ----RSSSRT  GFVGCGNTYS  VGPTFVSSSV  QNIDNTHQLQ  GSNPVLPNGM  SVVPRRSCVG  905
     Smed_Bcat1_ABW79875.1  LINQTGNSEI  AMRHFKQMGS  INISNECVN-  QDVQKAY---  ----------  ----------  893
                                                 1,100                               1,120                               1,140
                                                   |                                   |                                   |
Hd_Bcat1_WMSIL1_LOCUS14475  ---GGGYMDT  QQGPPPQGGP  M-TSPNPRGC  YSTTAP----  ---SSMDTT-  NSTNGYASPG  1014
 Em_Bcat1_EmuJ_001007700.1  ---AGGYIEP  QQ-PPPQAGP  M-TSPNPRAC  YPTNTP----  ---SSMDTT-  TSTSGYTSPG  1000
     Sm_Bcat1_Smp_023550.1  SISSSGYLSP  -------GGD  MFLNPSPSEY  KPFHEDNQGI  LRSSLLDQQ-  THTASISSPA  957
     Smed_Bcat1_ABW79875.1  --SNSSFKSP  SSHSLSVSGN  L--------C  SSNENSKKDM  MDVCMLDADW  IETCSDFSQG  943
                                                 1,160                               1,180
                                                   |                                   |
Hd_Bcat1_WMSIL1_LOCUS14475  TASRMAMGDD  YMT--PVMET  TMKPSVNPST  PNSTSSSGNQ  PDHRWFSSAQ  MCLP  1066
 Em_Bcat1_EmuJ_001007700.1  TAGRMALGDD  FMTGTPVLDG  GVKPSANPST  P---TSSGAP  PDHRWFSSAQ  MCLP  1051
     Sm_Bcat1_Smp_023550.1  IPSRNV----  ----------  ----NAGYLS  PDLMALEETD  PD--WFGGPA  VM--  989
     Smed_Bcat1_ABW79875.1  HSQKS-----  ----------  ----------  ----------  ----W----S  PINK  954
```

B

```
                                  α  α   α          α    α   α  α  α   α
Human_CTNB1_sp|P35222.1|  TNVQRLAEPS  QMLKHAVVNL  INYQDD

Smed_Bcat2_ABW79874.1  SSMIRMQKPA  QRLRFLVTNM  IDYIED
Em_Bcat2_EmuJ_001103600.1  FAVQRLSPCI  ESLTKAIGMI  INFKDD
Hd_Bcat2_WMSIL1_LOCUS880.1  SAVLRLSPCI  SNLAKAIGMV  INFKD

Smed_Bcat1_ABW79875.1  ADVSLSACYD  NKDENNRNPD  FGIDID
Em_Bcat1_EmuJ_001007700.1  SEVTGMTCSR  SDATMDIRGN  KISDLD
Hd_Bcat1_WMSIL1_LOCUS14475  SEISSMTCSR  SDATMDPRGN  KISDLD
```

Figure S5

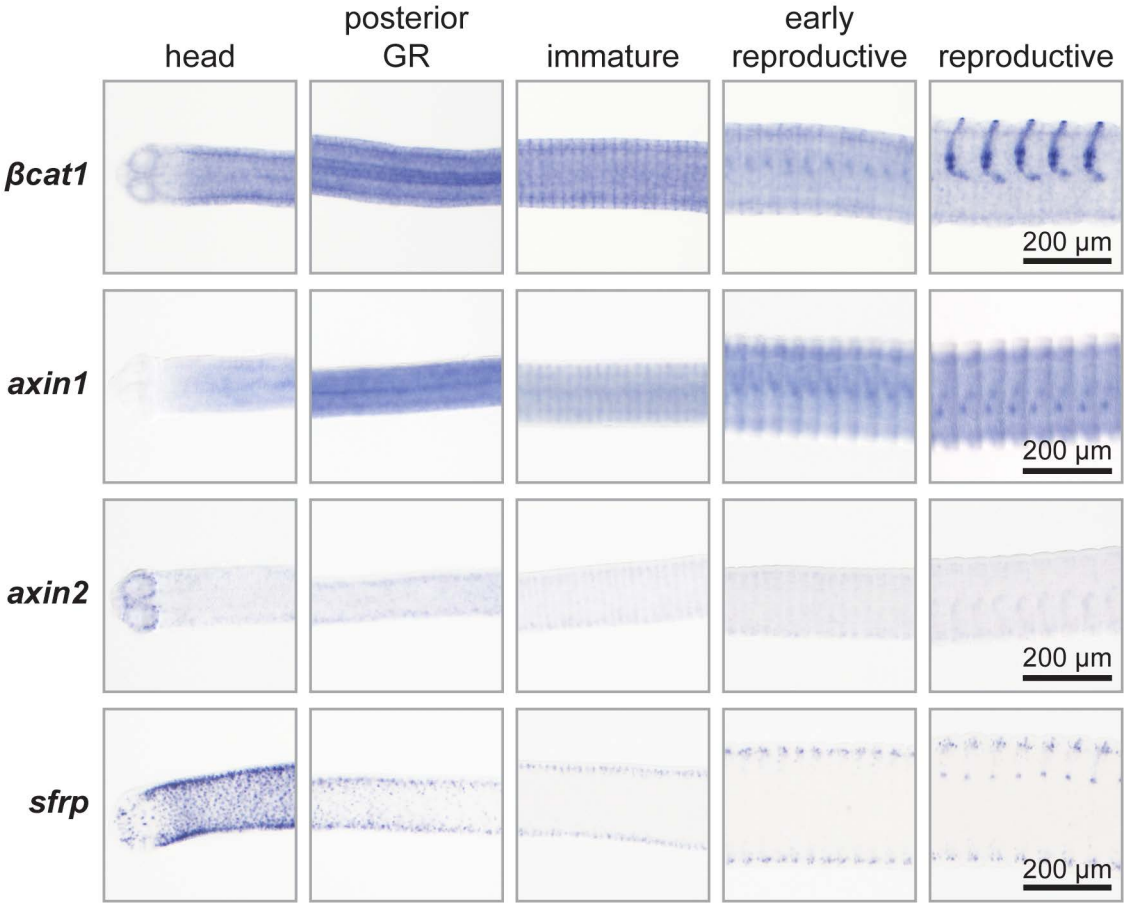
head
posterior GR
immature
early reproductive
reproductive
βcat1
axin1
axin2
sfrp
200 µm
200 µm
200 µm
200 µm

Figure S6

```
                                                  20                      40                      60
                                                   |                       |                       |
Hd_sfrp_HD_tophat_13573   M---------  ----LYLLLL  IFIAITSRGN  TVGRWDWNR-  ---VNKTSVT  TAPFGGGAFG  43
Em_sfrp_EmuJ_000838700.1  M---------  ----LPLVIL  FAIS-AAQAN  TVGRWDWHRG  GGAKNKTAVT  SSPFGGTSLS  46
Smed_sfrp1_ABY85212.1     MEMTKI----  ----FPLSLL  LFISNV----  ----------  ----------  ----------  18
Human_SFRP1_sp|Q8N474.1|  MGIGRSEGGR  RGAALGVLLA  LGAALLAVGS  ----------  ----------  ----------  30
Human_SFRP5_sp|Q5T4F7.3|  MRAAAAGGGV  RTAALALLL-  -GALHWAPAR  ----------  ----------  ----------  28
Human_SFRP2_sp|Q96HF1.2|  MLQGPG----  -----SLLLL  FLASHCCLGS  ----------  ----------  ----------  21

                                                  80                     100                     120
                                                   |                       |                       |
Hd_sfrp_HD_tophat_13573   RLTTADADMI  SNEPPQSPYF  SDWNRLVSG-  -YGSQ-RCYK  IPKELKLCHK  IGYDLMVLPN  100
Em_sfrp_EmuJ_000838700.1  RLTTADVHMI  SNEPPQSPYF  SDWNRLVSG-  -YGSQ-RCYK  IPRGMKLCHK  IGYDFMVLPN  103
Smed_sfrp1_ABY85212.1     ----------  ------NSFI  GDWQAFQSG-  -YTID-QCYQ  IPDNFTLCSN  VGYRLMVLPN  59
Human_SFRP1_sp|Q8N474.1|  ----------  ASEYDYVSFQ  SDIGPYQSGR  FYTKPPQCVD  IPADLRLCHN  VGYKKMVLPN  80
Human_SFRP5_sp|Q5T4F7.3|  ----------  CEEYDYYGWQ  AE--PLH-GR  SYSKPPQCLD  IPADLPLCHT  VGYKRMRLPN  75
Human_SFRP2_sp|Q96HF1.2|  ----------  ARGLFLFG-Q  PDF-------  SY-KRSNCKP  IPANLQLCHG  IEYQNMRLPN  62
```

Frizzled domain

```
                                                 140                     160                     180
                                                   |                       |                       |
Hd_sfrp_HD_tophat_13573   SLEHEGMDEV  ITQSEVWLTL  VNLGCHDELE  RFLCSLYAPV  CIRGYHEKLI  QPCRELCESV  160
Em_sfrp_EmuJ_000838700.1  SLEHETLDEA  ITQSEVWLTL  VNLGCHDELK  RFLCSLYAPV  CINGYHEKLI  QPCRELCESV  163
Smed_sfrp1_ABY85212.1     YIQHESIEEA  AQHSKVWMGL  VNTQCHVDIK  KFICSLYAPV  CISNQRNQKV  PPCRELCVTV  119
Human_SFRP1_sp|Q8N474.1|  LLEHETMAEV  KQQASSWVPL  LNKNCHAGTQ  VFLCSLFAPV  CLD----RPI  YPCRWLCEAV  136
Human_SFRP5_sp|Q5T4F7.3|  LLEHESLAEV  KQQASSWLPL  LAKRCHSDTQ  VFLCSLFAPV  CLD----RPI  YPCRSLCEAV  131
Human_SFRP2_sp|Q96HF1.2|  LLGHETMKEV  LEQAGAWIPL  VMKQCHPDTK  KFLCSLFAPV  CLDDL-DETI  QPCHSLCVQV  121

                                                 200                     220                     240
                                                   |                       |                       |
Hd_sfrp_HD_tophat_13573   RAACLPTMTT  FGLGWPDIVK  CSKFPQAPQE  LCIPPNKQRN  KTVVLKPETR  -CSGCVDKPT  219
Em_sfrp_EmuJ_000838700.1  RAACLPTMTT  FGLGWPDIVK  CSKFPQAPQE  LCIPLNKHKN  KTIILNPETR  -CSGCIDRPT  222
Smed_sfrp1_ABY85212.1     KESCLPSMKM  YGFDWPTIMK  CSKFPQFKNS  LCIP------  K-VV--PGKK  -CDLCMKIAS  170
Human_SFRP1_sp|Q8N474.1|  RDSCEPVMQF  FGFYWPEMLK  CDKFP--EGD  VCIAMTPPNA  TEASKPQGTT  VCPPCDNELK  194
Human_SFRP5_sp|Q5T4F7.3|  RAGCAPLMEA  YGFPWPEMLH  CHKFPL-DND  LCIAVQFGHL  P-ATAPPVTK  ICAQCEMEHS  189
Human_SFRP2_sp|Q96HF1.2|  KDRCAPVMSA  FGFPWPDMLE  CDRFPQ-DND  LCIPLASSDH  LLPATEEAPK  VCEACKNKND  180
```

Netrin domain

```
                                                 260                     280                     300
                                                   |                       |                       |
Hd_sfrp_HD_tophat_13573   YES-AIGSFC  TADVAVRSKV  LDLIPVPSTK  GQNTTYRIRT  DGRGGIFKM-  ---PKNVNKE  274
Em_sfrp_EmuJ_000838700.1  YES-AIGSFC  TADVVIRAKV  LDLVPTLPSS  GHNTTHRIRT  TGRVGAFKL-  ---PKTLNSI  277
Smed_sfrp1_ABY85212.1     YEV-IANRFC  LSPIVIRAKI  KRIIP---TS  GN--AIQIIL  QKKSKFLKF-  ---QANFSQN  220
Human_SFRP1_sp|Q8N474.1|  SEA-IIEHLC  ASEFALRMKI  KEV-----KK  ENGDKKIV--  PKKKKPLKLG  PIKKKDLKKL  246
Human_SFRP5_sp|Q5T4F7.3|  ADG-LMEQMC  SSDFVVKMRI  KEI-----KI  ENGDRKLIGA  QKKKKLLKPG  PLKRKDTKRL  243
Human_SFRP2_sp|Q96HF1.2|  DDNDIMETLC  KNDFALKIKV  KEI-----TY  INRDTKIILE  TKSKTIYKLN  GVSERDLKKS  235

                                                 320                     340                     360
                                                   |                       |                       |
Hd_sfrp_HD_tophat_13573   A-NLDFRMTC  DCPIIKAAMT  RSKGPGRWLL  MGKLNEDGRS  VTVLHLSQPS  RQNKGIKRAI  333
Em_sfrp_EmuJ_000838700.1  V-NLEFEMEC  DCPIIRAALT  RQKGPGRWLM  MGKLNDDRRT  VTVQHISQPS  RQNAGIKRAI  336
Smed_sfrp1_ABY85212.1     A--LELNLKC  NCTNLKFKQR  ALKG--RWII  MAQIDSDNKA  V-VNFISKWK  RKKAEFKHSM  275
Human_SFRP1_sp|Q8N474.1|  VLYLKNGADC  PCHQLDNLS-  -----HHFLI  MGR--KVKSQ  YLLTAIHKWD  KKNKEFKNFM  298
Human_SFRP5_sp|Q5T4F7.3|  VLHMKNGAGC  PCPQLDSLA-  -----GSFLV  MGR--KVDGQ  LLLMAVYRWD  KKNKEMKFAV  295
Human_SFRP2_sp|Q96HF1.2|  VLWLKDSLQC  TCEEMNDIN-  -----APYLV  MGQ--KQGGE  LVITSVKRWQ  KGQREFKRIS  287

                                                 380                     400                     420
                                                   |                       |                       |
Hd_sfrp_HD_tophat_13573   KEMRHQPDTL  CKVDLTRSSP  VVHPRTVAGR  PAANGAQISQ  EQKQQHQQLQ  PRRNGSNLSK  393
Em_sfrp_EmuJ_000838700.1  RDIRRRPDSL  CKVDLMHPNP  VAHSRAISSL  SSPSSMQSLR  PRSHQSRRYR  P-----HLSP  391
Smed_sfrp1_ABY85212.1     KIIQNFGHIV  CKSKLPDGIS  L-RERYAAYL  KMNNQLKYSN  ERKLQTRKFR  ---------K  325
Human_SFRP1_sp|Q8N474.1|  KKMKNHE---  CPTFQSVF--  ----K-----  ----------  ----------  ----------  314
Human_SFRP5_sp|Q5T4F7.3|  KFMFSYP---  CSLYYPFFYG  AAEPH-----  ----------  ----------  ----------  317
Human_SFRP2_sp|Q96HF1.2|  RSIRKLQ---  C---------  ----------  ----------  ----------  ----------  295

                                                 440                     460                     480
                                                   |                       |                       |
Hd_sfrp_HD_tophat_13573   EERRRRRQLR  RRRNE---AG  AQQQQHPSNV  TLSSTNSQES  QQPVNDMPIG  VNTQHPYNQQ  450
Em_sfrp_EmuJ_000838700.1  EERRRR-QLR  RRRNHPRGSS  PEAQQRAANV  TPSRKPPQLQ  QQPINDIPIL  TPTPRPFSHH  450
Smed_sfrp1_ABY85212.1     QKSRK-----  ---------S  VKPNNRSAGI  S---------  ----------  ----------  342
Human_SFRP1_sp|Q8N474.1|  ----------  ----------  ----------  ----------  ----------  ----------  314
Human_SFRP5_sp|Q5T4F7.3|  ----------  ----------  ----------  ----------  ----------  ----------  317
Human_SFRP2_sp|Q96HF1.2|  ----------  ----------  ----------  ----------  ----------  ----------  295
```

Figure S7

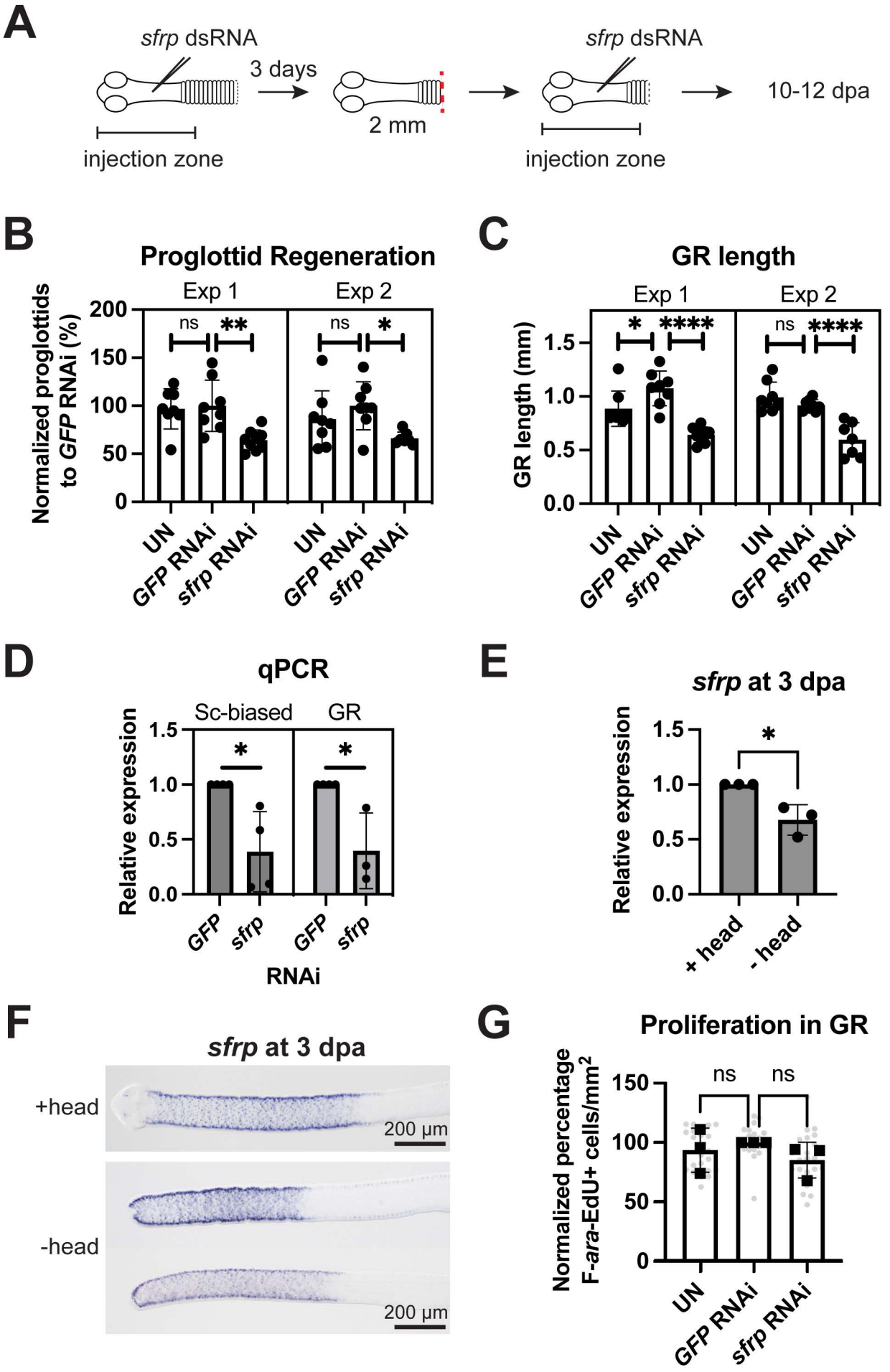
A
sfrp dsRNA
3 days
2 mm
sfrp dsRNA
10-12 dpa
injection zone
injection zone
B
Proglottid Regeneration
Exp 1
Exp 2
Normalized proglottids to GFP RNAi (%)
200
150
100
50
0
ns
**
ns
*
UN
GFP RNAi
sfrp RNAi
C
GR length
Exp 1
Exp 2
GR length (mm)
1.5
1.0
0.5
0.0
*
****
ns
****
UN
GFP RNAi
sfrp RNAi
D
qPCR
Sc-biased
GR
Relative expression
1.5
1.0
0.5
0.0
*
*
GFP
sfrp
GFP
sfrp
RNAi
E
sfrp at 3 dpa
Relative expression
1.5
1.0
0.5
0.0
*
+ head
- head
F
sfrp at 3 dpa
+head
-head
200 µm
200 µm
G
Proliferation in GR
Normalized percentage F-ara-EdU+ cells/mm2
150
100
50
0
ns
ns
UN
GFP RNAi
sfrp RNAi

Figure S8

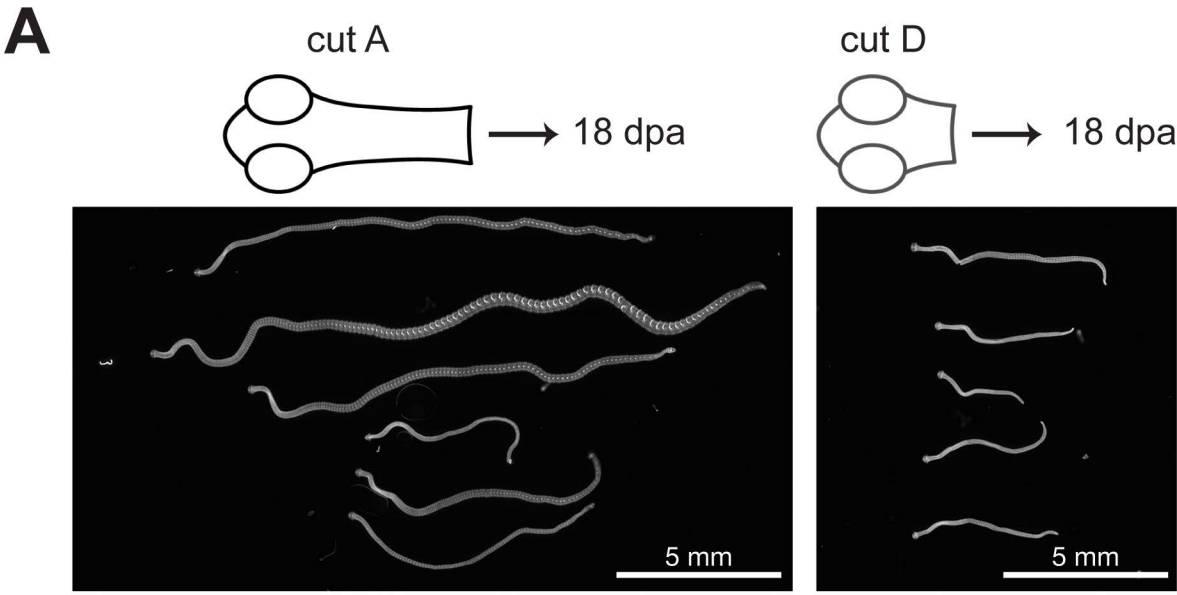
A
cut A
18 dpa
cut D
18 dpa
5 mm
5 mm

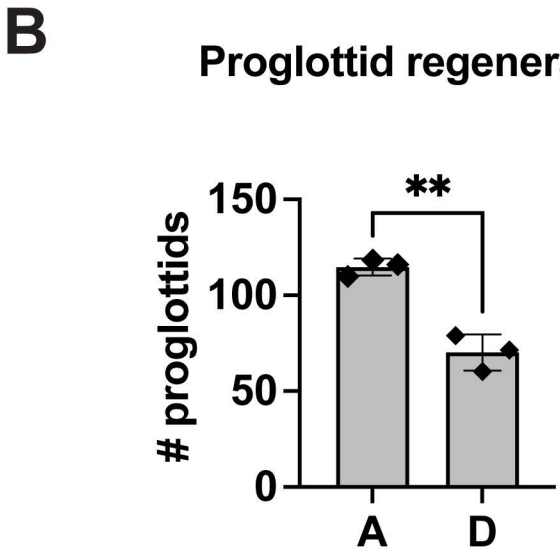
B
Proglottid regeneration
proglottids
150
100
50
0
**
A
D